Annals of Glaciology

Article

Cite this article: Liu X, An L, Hai G, Xie H, Li R (2024). Updating glacier inventories on the periphery of Antarctica and Greenland using multi-source data. *Annals of Glaciology* 1–18. https://doi.org/10.1017/aog.2023.75

Received: 29 December 2022
Revised: 17 November 2023
Accepted: 20 November 2023

Keywords:
glacier mapping; ice cap; mountain glaciers; remote sensing

Corresponding author:
Lu An;
Email: Anlu2021@tongji.edu.cn

Updating glacier inventories on the periphery of Antarctica and Greenland using multi-source data

Xingchen Liu, Lu An, Gang Hai, Huan Xie and Rongxing Li

Center for Spatial Information Science and Sustainable Development Applications, College of Surveying and Geo-informatics, Tongji University, Shanghai, China

Abstract

Melting and calving of glaciers and ice caps in Antarctica and Greenland could potentially contribute significantly to global sea level rise. Updates to existing outlines that provide critical glacier baseline information in both regions could help in the analysis of particular changes in glacier parameters such as area and volume from time-series inventories. Here we synthesize previously established techniques and apply new multi-source datasets to update glacier outlines in selected test areas of Antarctica and Greenland, as well as to reduce uncertainties and errors during the mapping process. The workflow includes mapping glacier boundaries, subdividing glaciers by watersheds and assigning glacier attributes. Complicated glacier scenarios and updating challenges in polar regions are discussed and demonstrated by representative case studies. For the first time in Antarctica, we analyze the effect of terminus types on mapped glacier areas, and in Greenland we compare the differences with glacier mapping results using Landsat OLI and ETM+. With new data sources, the methods described in this study might help to create glacier outlines on a larger scale in Antarctica and Greenland. Although data sources can be substituted, the enormous amount of manual labor required to update glacier inventories remains a significant challenge.

1. Introduction

Glaciers are important indicators for climate change assessment because they are very sensitive to climate variability (Oerlemans, 2001). Most of the global glacier volume is contained in the two polar ice sheets and the glaciers and ice caps (GIC) that surround the ice sheets (Frezzotti and Orombelli, 2014). Mass loss of GIC in Antarctica and Greenland has contributed to global sea level rise, with more potential in the future (e.g. Meier and others, 2007; Hock and others, 2009; Gardner and others, 2013; Zemp and others, 2019; Hugonnet and others, 2021). Glacier inventories provide important baseline data for determining specific changes of glacier area/volume and contribution to sea level in response to climate change (Rastner and others, 2012). Investigation of glacier variability requires a multi-period inventory, and accurate determination of their attributes requires accurate mapping of glacier boundaries and subdivision of glacier complexes into individual glaciers.

The Global Land Ice Measurements from Space initiative (GLIMS; National Snow and Ice Data Center (NSIDC), 2022) aims to collect the derived outlines of the world's glaciers, record and store geospatial information about glaciers, and analyze glacier extent and change (Raup and others, 2007). There are two GLIMS vector databases with complete content and comprehensive coverage that provide detailed two-dimensional (2D) outlines and attribute information for GIC in Antarctica and Greenland:

Antarctica: Bliss and others (2013) compiled an inventory of GIC on the periphery of Antarctica (Fig. 1a), excluding ice rises. Glacier outlines (1957–2005) were derived primarily from manually created polygon files representing coastlines and rock areas from the Antarctic Digital Database (ADD; https://www.add.scar.org/). Watersheds of glaciers were created from previous digital elevation models (DEMs; e.g. Radarsat Antarctic Mapping Project (RAMP) DEM; https://nsidc.org/data/nsidc-0082/versions/2; Liu and others, 2015). Since the island glaciers were considered separate from the continental ice sheet (Hock and others, 2022), connectivity levels (CLs) of glaciers in this region should theoretically be all CL0 (i.e. no connection).

Greenland: Rastner and others (2012) compiled an inventory of local GIC in Greenland (Fig. 1b). They presented the first comprehensive inventory of Greenland GIC based on semi-automatic glacier mapping techniques and Landsat scenes (most ETM+ scenes from 1999 to 2002), mainly using the Greenland Ice sheet Mapping Project (GIMP) DEM (https://nsidc.org/data/nsidc-0645/versions/1; Howat and others, 2015) for watershed analysis and glacier division. Meanwhile, the inventory defines the CL of each glacier with the ice sheet (i.e. CL0; CL1: weak connection (clearly separated by drainage divides in the accumulation region, unconnected or only in contact in the ablation region); CL2: strong connection (difficult to

https://doi.org/10.1017/aog.2023.75 Published online by Cambridge University Press

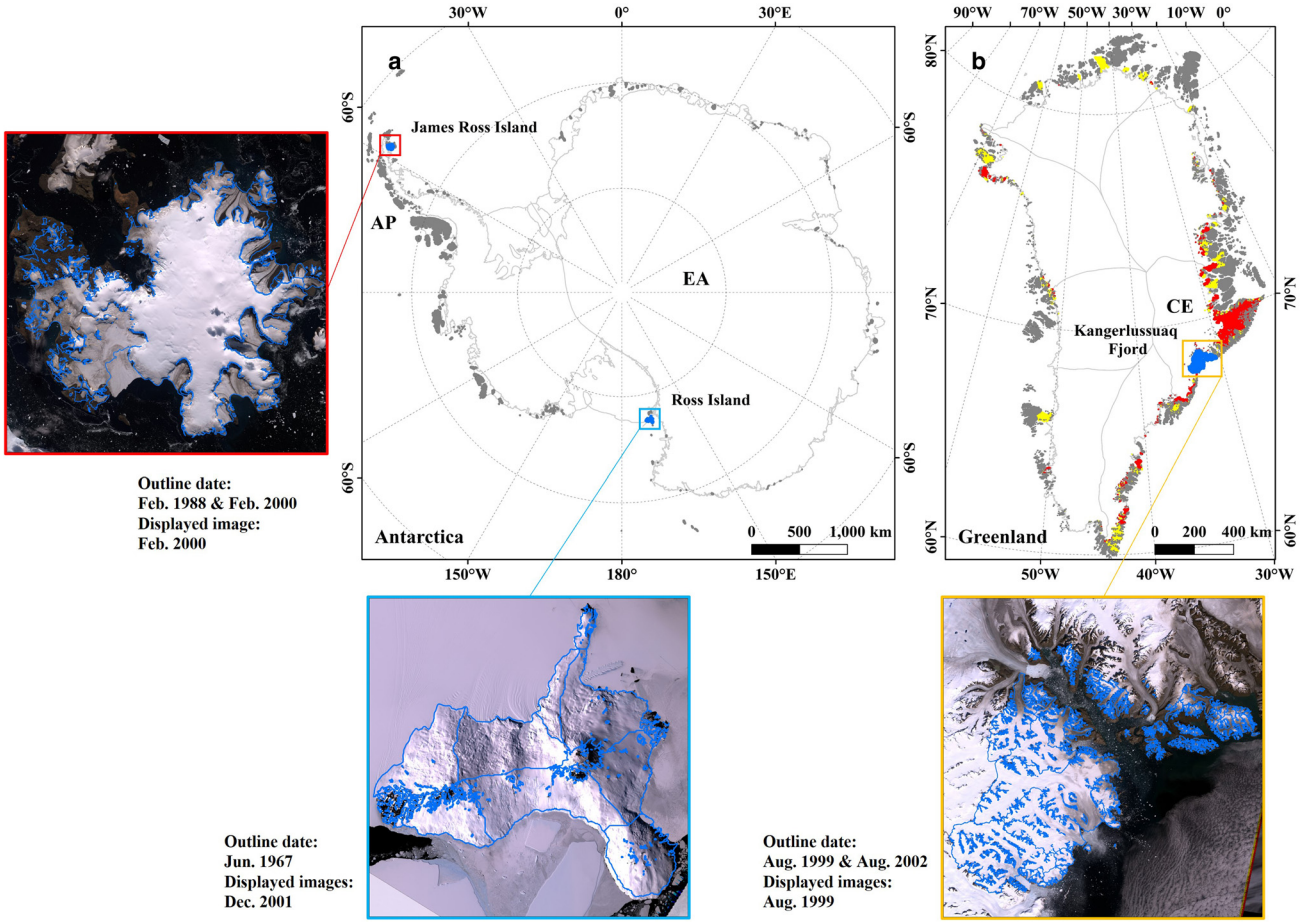

Figure 1. Previous inventories and regional coverage map of GIC in Antarctica and Greenland (CL0: dark gray; CL1: yellow; CL2: red). The boxes show the locations of test areas for updating glacier outlines for the new period in this study. The enlarged images show the previous glacier outlines from RGI 6.0 in test areas.

separate in the accumulation region and/or converge in the ablation region)) (Rastner and others, 2012).

These inventories fill important gaps in the Randolph Glacier Inventory (RGI) 6.0, which is a one-time snapshot of global glaciers that is supplemental to the multi-temporal database of GLIMS (Pfeffer and others, 2014), and help to analyze the specific characteristics of these glaciers and model the associated impacts to determine the mass balance of glaciers individually or globally, as well as their impacts on sea level rise (e.g. Huss and Farinotti, 2012; Bolch and others, 2013; Gardner and others, 2013; Zemp and others, 2019; Hugonnet and others, 2021).

So far, only a few studies have investigated localized GIC changes in Antarctica and Greenland from the standpoint of glacier inventory (e.g. Jiskoot and others, 2012; Cook and others, 2014). For the last two decades, complements to these inventories have been lacking due to the high workload required for creating such datasets. Although the inventory of GIC around the Antarctic Peninsula (AP) has been updated, their source date is still limited to 2000–02 (Huber and others, 2017). There are some updates for parts of the regions on the periphery of Greenland and Antarctica in the just released RGI 7.0 (RGI Consortium, 2023), but most glaciers have not been updated from the well-known RGI 6.0. Updating or creating accurate glacier outlines is extremely difficult in polar areas, as glaciers with all CLs in Greenland and glaciers discharging into ice shelves in Antarctica, as well as ice-debris landforms, are common. Some of these challenges have been discussed (e.g. Paul and Kääb, 2005; Rastner and others, 2012; Bliss and others, 2013), in general, there is still a lack of detail and clarity on the mapping challenges and their solutions for complex polar regions, especially in Antarctica.

Although previous glacier inventories have been established, existing techniques, such as the use of coherence images and ice velocity maps to support the glacier mapping, had not been effectively applied at the time of their creation. The positioning accuracy and resolution of the source material limit the accuracy of individual glacier outlines, and it is unclear how improved positioning, vertical accuracy and spatial resolution of remote-sensing data used in Antarctica and Greenland could facilitate the definition of improved glacier inventories there. Furthermore, the impact of terminus types and sensor types on polar glacier mapping results is rarely studied, even if it may introduce an uncertainty in updating results and future analysis in glacier change. Another question is whether existing datasets can help in the task of updating glacier inventories.

This study presents a detailed demonstration of selected case studies to better understand the above difficulties and help update glacier inventories in Antarctica and Greenland. We synthesize existing techniques and new source data to update the inventories of selected GIC for new time periods, which are located at the periphery of the two ice sheets. We update a glacier inventory using a well-established workflow that includes mapping glacier boundaries, subdividing glaciers by watersheds and assigning attributes. The mapping solutions for complex glacier scenarios are discussed and the precision or uncertainty of glacier outlines is evaluated, taking James Ross Island beside the AP, Ross Island in East Antarctica (EA) and the glacier scene around Kangerlussuaq Fjord in central east (CE) Greenland as test regions (Fig. 1). We compare the results and methods to

https://doi.org/10.1017/aog.2023.75 Published online by Cambridge University Press

the previous inventory in these regions. We also highlight the challenges in upscaling these techniques in order to complete full inventories in the study area.

2. Source data

In view of updating the GIC inventories in the study areas, it is necessary to consider the reliable remote-sensing data that are available for the analysis period (i.e. last two decades). The source data information used in the applications and discussions of this study is listed in Tables S1–S3.

2.1 Optical images

Medium- to high-resolution optical satellite sensors such as Landsat 4/5 TM, Landsat 7 ETM+, Landsat 8 OLI and ASTER are commonly used for mapping glaciers (Winsvold and others, 2016). However, the small image extent of ASTER (60 × 60 km) limits its ability to map glaciers over a large region in the study area, especially in Greenland, where the optimal threshold for ratio images in the semi-automatic mapping method must be selected for each scene. The Landsat image archive represents the longest continuous satellite record and has sufficient resolution to track glacier changes, making it useful for glacier mapping (Winsvold and others, 2016). Landsat Level 1 T (L1 T) satellite imagery with resolutions up to 30 m (multispectral) or 15 m (panchromatic) was used to update glacier inventories in test areas. This dataset is available on the United States Geological Survey (USGS) Earth Explorer website, and its T1-level data provide consistent geographic calibration within prescribed tolerances (<12 m root mean square error (RMSE); https://earthexplorer.usgs.gov/). The presence of striping problems in ETM+ scenes after 2003 due to the scan line corrector affects the mapping of glaciers, so we primarily used Landsat 8 OLI to map glaciers since 2013. We selected less cloudy images taken during summer time in Antarctica and Greenland to obtain sufficient light for the scenes and to reduce the impact of seasonal snow on glacier mapping. To further exclude clouds, snow and shadows and to fully represent and accurately map the glaciers, we referenced multiple images alternately. OLI bands 6, 5 and 4 were each used in RGB (red, green, blue) channels, respectively, to generate contrast-enhanced false-color composites to help correctly identify glaciers (Paul and others, 2015).

The correction for seasonal snow is a challenge for creating glacier inventories, regardless of the manual or automatic method used. It is not recommended to use scenes covered by seasonal snow for mapping (Paul and others, 2015), and satellite scenes at the end of the ablation season should be selected if possible (Paul and others, 2009; Racoviteanu and others, 2009). In addition, snow may still fall during summer in the study area. Given these limitations, image selection is always a challenge. Fortunately, in the case of infrequent updates, Landsat OLI offers the opportunity to select better data scenes from the last decade.

The optical data in Google Earth, which come from optical sensors such as QuickBird and Worldview, can be very high-resolution (better than 1 m) (Molg and others, 2018) and allows for viewing from a three-dimensional (3D) perspective. Therefore, they were used in this study as quality control and accuracy verification for glacier mapping if available. The Landsat Image Mosaic of Antarctica (LIMA; https://lima.usgs.gov/; Bindschadler and others, 2008) and the New Image Mosaic of Greenland (http://data.tpdc.ac.cn/; Chen and others, 2020) serve as a background for orientation in this study. These mosaics are mainly composed of Landsat 7 ETM+ and Landsat 8 OLI imagery and allow us to quickly locate glaciers in the study area.

2.2 Coherence images

Interferometric synthetic aperture radar (InSAR) coherence can be used to accurately map debris-covered glacier margins and is almost independent of weather and solar illumination (Atwood and others, 2010; Ke and others, 2016). InSAR coherence represents the complex correlation between two SAR images and indicates the temporal stability of the backscattered signal, and thus can be used to separate stable and unstable surface regions (Lippl and others, 2018). When most of the seasonal snow has disappeared during summer, glacier flow and melting are responsible for most of the surface-geometry changes, resulting in very low coherence (Frey and others, 2012).

Designed for SAR interferometry applications and displacement monitoring, the Copernicus Sentinel-1 constellation provides free access to SAR images of the same orbit every 12 days over the study area (Strozzi and others, 2020). In this study, radar data were chosen from the C-band Sentinel-1A and -1B sensors with interferometric wide swath mode (IW) to estimate glacier coherence for the new period. We selected the original SAR single-look complex (SLC) pairs and acquired terrain-corrected and geocoded coherence images processed by the Alaska Satellite Facility (ASF; https://search.asf.alaska.edu/) using GAMMA software and the best publicly available global DEM (Copernicus DEM; 30 m). The 10 × 2 number of looks was selected to obtain products with a pixel spacing of 40 m.

In the case studies, interferograms during summer time were selected to maximize decoherence on glaciers, where surface melting rapidly reduces coherence on the glacier (Atwood and others, 2010). However, additional glacial indicators in coherence and surface slope are needed to extract decoherence areas and filter out low coherence caused by steep terrain, respectively (e.g. Atwood and others, 2010; Ke and others, 2016; Lippl and others, 2018). We tuned and determined these thresholds to minimize the holes within glaciers and to achieve the fit with most of the confirmed ice pixels in optical scenes. Although water bodies also lead to very low coherence, they can be clearly distinguished in the optical images (e.g. Frey and others, 2012).

2.3 DEMs and ice velocity maps

DEMs can be used for semi-automatic definition of glacier divisions based on flow direction grids and watershed analysis, and for determining glacier attributes (Paul and others, 2009; Racoviteanu and others, 2009). The Reference Elevation Model of Antarctica (REMA; Howat and others, 2019) and ArcticDEM (Porter and others, 2018) were derived from hundreds of thousands of individual stereo DEMs registered vertically to Cryosat-2 and ICESat altimetry, with absolute uncertainties of less than 1 m and relative uncertainties of decimeters over most of the area (https://www.pgc.umn.edu/data/). In the case studies, we used mosaics of these two high-precision DEMs as inputs to generate contours, slope, aspect and flow-direction maps to support the accurate definition of glacier boundaries and watersheds. These mosaics have a 32 m resolution which have essentially the same spatial resolution and are within the same decade as the optical images (Paul and others, 2009). In previous inventories, the RAMP DEM has a reported vertical accuracy of about 100–130 m and a horizontal resolution of 200 m in rugged mountainous areas (Liu and others, 1999), and the GIMP DEM with 90 or 30 m resolution and reported vertical accuracy of about 10 m was used (Rastner and others, 2012; Howat and others, 2014). In particular, REMA provides unprecedented resolution and accuracy for Antarctica and the potential to improve the accuracy of glacier inventories.

The delineation of glacier drainage basins at gentle slopes in the study area is challenging because of the accompanied local

https://doi.org/10.1017/aog.2023.75 Published online by Cambridge University Press

topographic disturbances and complex ice movement patterns (e.g. Krieger and others, 2020b). Therefore, to supplement DEM data, we additionally used ice velocity maps from SAR data for Antarctica (https://nsidc.org/data/nsidc-0484/versions/2; Rignot and others, 2017) and Greenland (https://nsidc.org/data/nsidc-0478/versions/2; Joughin and others, 2015) to guide glacier division. The direction of ice flow may indicate a different direction than the aspect due to glacier instability, bedrock features and ice volume interactions (Krieger and others, 2020a). In addition, the magnitude of the ice velocity indicates intuitively its acceleration from the accumulation zone to the ablation zone, thus assisting in delineating the individual glacier extent.

3. Methods

Glacier outline generation involves three main steps: (1) mapping glacier boundaries, (2) delineating glacier divides and (3) assigning glacier attributes (Fig. 2). All calculations are performed using ArcGIS version 10.5 and ENVI version 5.3 with various toolboxes available. The type of map projection of the layers is 'WGS84 Antarctic Polar Stereographic' in Antarctica and 'WGS84 NSIDC Sea Ice Polar Stereographic North' in Greenland. Figure 2 illustrates our technical workflow, and the three main steps are described in more detail in the following sections.

3.1 Mapping of glacier boundaries

In Antarctica, individual glaciers can be very large (up to 6000 km^2) and their terminus characteristics are unique (Bliss and others, 2013). A large fraction of glaciers share a common boundary with ice shelves (Fig. 3a). However, the same spectral properties prevent automatic classification methods from separating them, implying that manual interpretation is necessary to map most or even the whole glacier boundary. The ocean terminus indicates that the glacier boundary line is coincident with the coastline and the land-terminating boundaries normally represent the peripheral retreat of island glaciers and the exposure of internal rocks (Fig. 3b). Automatic classification methods are well applicable to extract land-terminating or marine-terminating glacier boundaries with less sea ice and seasonal snow influence in Antarctica. This is the case for Greenland, where most glaciers terminate on land (Fig. 3c), and some ice caps (e.g. Flade Isblink ice cap) and narrow outlet glaciers are marine-terminating (Fig. 3d). Glaciers are generally clearly separated from the land and ocean during the melting period, so that initial glacier boundaries can be automatically derived to facilitate manual correction (e.g. Rastner and others, 2012).

Greenland has extensive debris cover over glacierized areas (Herreid and Pellicciotti, 2020), which poses a significant mapping challenge. In contrast, most Antarctic glaciers are ice caps, which means that there is generally no debris that can fall from the rock walls onto the glacier (the glacier scenario on James Ross Island in Case Study 2 is an exception). The current climatic circumstances, which include sustained subfreezing conditions and a lack of diurnal circulation, reduce the amounts of debris produced by freeze–thaw activity. Therefore, the largely debris-free conditions make the classification of nunataks contained within the glacier possible (e.g. Burton-Johnson and others, 2016).

To overcome the ground conditions and mapping challenges in glacial regions, manual interpretation and well-established automatic methods were combined to extract glacier boundaries.

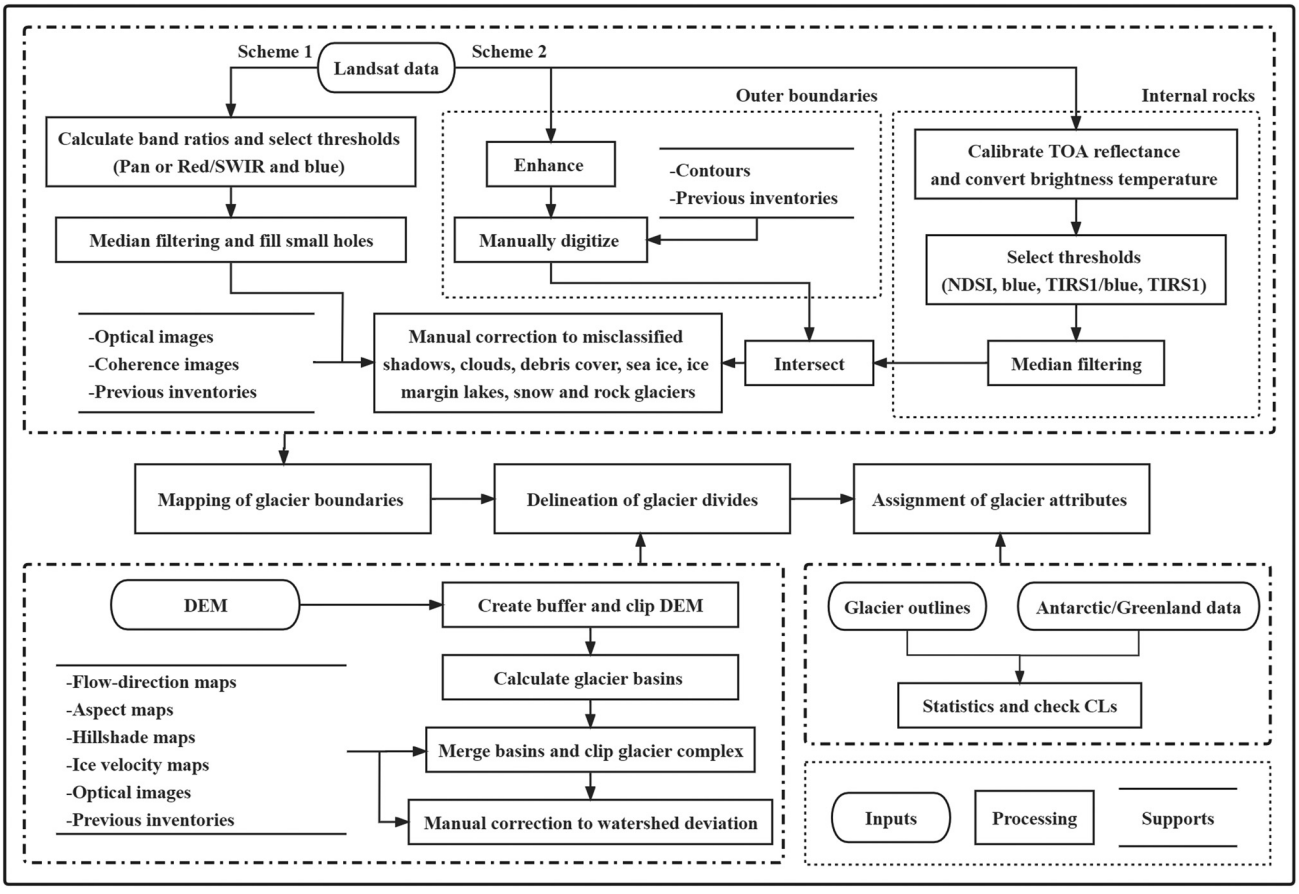

Figure 2. Framework for updating glacier inventories in this study, including three modules (mapping of glacier boundaries, delineation of glacier divides and assignment of glacier attributes).

https://doi.org/10.1017/aog.2023.75 Published online by Cambridge University Press

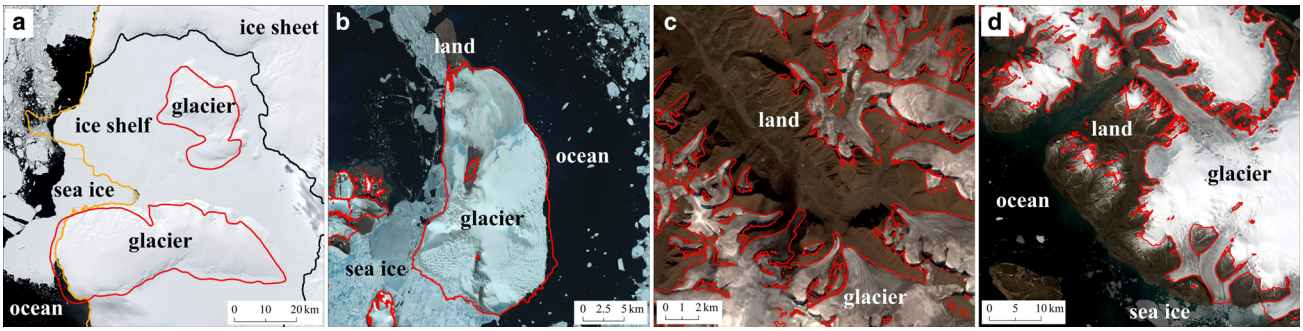

Figure 3. Examples of terminus characteristics of glaciers in the study areas. The red glacier boundaries are from RGI 6.0, with Landsat OLI scenes in (a) West Antarctica (WA) (72.8°S, 90.4°W), (b) AP (64.5°S, 57.2°W), (c) central west (CW) of Greenland (69.9°N, 53.6°W) and (d) northwest (NW) of Greenland (76.8°N, 69.3°W). The orange and black lines in (a) represent the coastlines and grounding lines, respectively.

Two schemes were considered to map glaciers that share different length proportion boundaries with ice shelves or sea ice. The difference between the two schemes is whether the visual interpretation method is best used for post-processing the automatically derived boundaries or for mapping the initial glacier outer boundaries. It should be noted that glacier boundaries can be visually interpreted in any case and the two schemes can be complementary to each other to cope with different glacier situations over a wide study area when taking into account the efficiency of polygon editing.

Scheme 1: The well-established semi-automatic band ratio method was adopted to map glaciers with a large proportion of land terminus and less sea ice attached ocean terminus (Case Studies 1 and 3). Glacier classification using threshold segmentation of the Landsat TM band raw data ratio (e.g. TM3/TM5) has proved to be the most effective method for mapping glaciers (Paul and others, 2002). The optimal ratio threshold should be found for each glacier scene (Rastner and others, 2012) and an additional threshold in the blue band can be introduced to improve the mapping of shaded glaciers, which have higher reflectance than bare rock (Paul and Kääb, 2005; Paul and Andreassen, 2009). We applied the scheme proposed by Paul and others (2016) to replace the 30 m spatial resolution red band (OLI4) with a 15 m resolution panchromatic band (OLI8) for glacier mapping (OLI8/OLI6) to automatically draw glacier boundaries at higher spatial resolution. To calculate the ratio, the spatial resolution of the OLI6 image was improved to 15 m by bilinear interpolation. A median filter (3 × 3 kernel) was applied to smooth the glacier boundary and this process is considered to have little influence on the final glacier areas (He and Zhou, 2022). However, higher resolution data are usually accompanied by higher processing workload (Paul and others, 2016), as more dirty ice, fine rock outcrops and debris-covered areas are identified in detail, causing many small holes in the glacier polygons. Therefore, the polygon part elimination tool in ArcGIS was additionally used to eliminate these extremely small holes (area <0.003 km^2) in the glacier polygons at an OLI resolution of 15 m to reduce the processing effort.

Scheme 2: Antarctic glaciers with ice shelves and marine-terminating boundaries attached to more sea ice were manually interpreted (Case Study 2). However, the raw imagery does not generally distinguish well between glaciers and ice shelves, making it difficult to visually interpret their demarcation lines. Therefore, to achieve sufficient discrimination between glaciers and ice shelves, the quality of each image was improved using appropriate methods (e.g. histogram equalization, GAMMA stretch). The (enhanced) images were then used to manually digitize the outer boundaries of glaciers. To reduce the subjectivity of visual interpretation in this process, the boundary mapping was simultaneously referenced to the REMA contours at the glacier boundary. This ensures that 2D glacier boundaries drawn based on imagery can also be well validated in terms of elevation. There have been some important advances in automatic detection of tidewater calving margins over the past decade (e.g. Lea and others, 2014; Cheng and others, 2021), but conservatively manual digitization was used to distinguish glaciers from sea ice, which is a simpler separation process. Once a glacier's outer boundary is delineated, exposed rocks present within the mask were identified and excluded in the next step. We referred to the automatic method of Burton-Johnson and others (2016) and used multispectral imagery with top-of-atmosphere (TOA) reflectance correction and brightness-temperature conversion to delineate rock outcrops that were contemporaneous with the imagery. The normalized difference snow index (NDSI) technique was used to identify sunlit rocks and blue reflectance threshold was selected to identify rocks in shadow. Separate thresholds (Thermal Infrared SenSor 1 (TIRS1) brightness temperature/blue reflectance, TIRS1 brightness temperature) were then applied to remove misclassified cloud pixels. The drawn glacier outer boundary was used as a mask to exclude the ocean and rock pixels beyond the glacier extent. We treated water and rock pixels within the glacier extent together as classifications different from ice and therefore did not use the threshold of normalized difference water index (NDWI). Finally, by smoothing the rock classification raster using a median filter, the created topological corner connections and pixel-sized data voids after the intersection of rock outcrops and outer boundaries can be effectively mitigated.

Although clean and slightly dirty glaciers were mapped accurately, manual corrections to misclassified shadows, clouds, debris cover, sea ice, ice margin lakes and snow were time consuming. The main challenges and solutions for updating the glacier outlines in test areas are described in the following.

Previous experience has shown that the effort required to correct snow areas after automatic mapping of clean ice can be enormous (Paul and others, 2015), and the distinction between snow and glaciers can be more challenging in cold study areas. However, this process will be easier when updates are made to existing inventories. In any case, as described in section 2.1, the selection of best images to map glaciers during the ablation season is of utmost importance. The following strategies were adopted to deal with potential snow conditions in the glacier scene. We applied a median filter and a glacier size threshold of 0.05 km^2 to help remove noise from small isolated snow patches. In optical images, snowfields normally present irregular features such as radial bars, and glaciers can be distinguished from them by visible crevasses, the existence of a visible toe and surface moraines (Howat and others, 2014). However, accurately differentiating between glaciers and perennial and seasonal snow remains a

https://doi.org/10.1017/aog.2023.75 Published online by Cambridge University Press

daunting task, even in high-resolution images of Google Earth (e.g. Bolch and others, 2010; Le Bris and others, 2011; Paul and others, 2011, 2017). At this point, we looked at multi-time (within a year or over multiple years) images (e.g. Lu and others, 2020) and used the best images to exclude seasonal snow (also for clouds and shadows), similar to the principle of using a time stack to synthesize the best mapping scenes (Winsvold and others, 2016). As an aid, we also identified snow by SAR coherence information. The isolated and fine features of snow patches make them typically blurred in coherence images. Despite potentially wet conditions, some SAR signal penetration in seasonal snow is possible (Winsvold and others, 2018). Although the simultaneous low coherence of snow and glaciers is not beneficial to determine, combining the penetration of SAR waves with the examination of coherence and optical information in the case studies, we suggest that the thin snow contaminating the optical mapping scene might exhibit higher coherence and possibly help exclude seasonal and perennial snow. The classification of snow from the previous inventories was also used as a reference for the decision.

Shaded glaciers were effectively corrected by increasing the brightness of the optical images. Coherence images also assist in mapping glaciers in deep shadow when using slope thresholds to exclude low coherence due to steep mountain slopes. In scheme 1, OLI band ratio reduces workload by providing accurate mapping in the shaded areas without the need to add a threshold in the blue band (Paul and others, 2016). However, when the image ratio is applied to a scene with larger coverage and more complex terrain, mapping of ice in shadows remains limited because a single threshold is insufficient to map shaded ice in both dark zones and slightly brighter zones. The latter appears brighter because it is on a broad snowfield in high terrain, with surrounding snow in sunlight creating diffuse reflection (Paul and others, 2017), whereas the former is generally in low-lying terrain and blocked by steep mountains. Accurate mapping of shaded ice in bright zones requires a high threshold for the OLI8/OLI6 ratio, while shaded and dirty ice in dark zones requires a low value (Fig. 4). Similarly, mapping of brightly shaded rocks requires a higher upper blue reflectance threshold than shaded rocks in darker areas in scheme 2. In this case, we alternately selected thresholds for accurately mapping shaded ice in dark or light zones even in a single scene. We manually created masks that could distinguish between bright and dark zones and separated them at locations where the classification results are insensitive to the threshold. These masks were used to crop one of the ratio images and mosaic the result over the other ratio image. The selection of masks and thresholds, depending on the actual scene, is always an optimization process and a trade-off between total amount of manual correction required for the range. We performed this work before converting the classification raster into a vector. The process of distinguishing between bright and dark scenes also takes time but could reduce the need for extensive corrections to the vectors.

In the absence of fieldwork, identifying ice-debris complexes (including rock glaciers, ice-cored moraines and debris-covered dead-ice bodies; Bolch and others, 2019) gives a great challenge to glacier interpreters, such as separating them from bedrock and flowing debris-covered glaciers. Another problem is that there is currently no clear definition of the characteristics that should be included in a glacier inventory. When earlier inventories blur these definitions, updating and creating glacier outlines becomes more difficult (i.e. interpretation differences must be considered). In previous work, Paul and others (2004) specified how debris cover should be handled during glacier mapping. Molg and others (2018) followed a more conservative interpretation when no clear boundary between debris-covered glaciers and rock glaciers could be found. In this study, we chose to exclude rock glaciers, bedrock and stable moraines without ice core melting or significant surface collapse from the inventory. We primarily rely on coherence information to categorize debris-covered glaciers and moraines that show signs of activity as glaciers, and refer to them collectively as debris-covered glaciers.

The debris covering a glacier has the same spectral properties as the surrounding terrain (Paul and others, 2004), meaning that the application of automatic delineation methods would lead to misclassification. We therefore combine optical images and coherence maps to map debris-covered glaciers. On a false-color composite (RGB in bands 654, respectively) of OLI images, debris cover typically shows a darker brown color than the surrounding land. In addition, typical features of debris-covered glaciers, such as distinctive tongues and the presence of melt water streams and small melt water ponds, contribute to their identification (Howat and others, 2014). Coherence images provide an accurate reference for mapping the edges of glacial tongues, either as raw images or with added coherence or slope thresholds (e.g. Atwood and others, 2010; Frey and others, 2012; Ke and others, 2016; Lippl and others, 2018). However, there is an uncertainty in discerning debris-covered glaciers by coherence in potentially changing landforms such as snow cover (Molg and others, 2018), so decorrelation on debris-covered glaciers must be separated from that caused by changes in the surrounding land cover (Barella and others, 2022). Therefore, the land cover type was first determined from multi-time and high-resolution optical images (e.g. Nuimura and others, 2015), and then changes were excluded as much as possible based on the optical images near

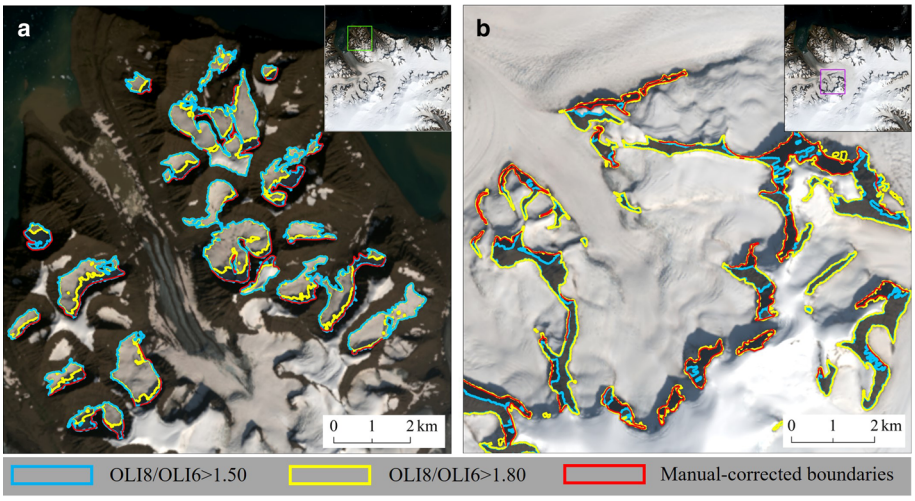

Figure 4. Shaded ice requires different thresholds for the OLI8/OLI6 ratio in dark and bright zones. The glacier scene is located in CE of Greenland (70.2°N, 25.0°W). (a) A low threshold (1.50) produces better results than a high threshold (1.80) for automatic mapping of shaded ice in dark zones. (b) A high threshold leads to better results than a low threshold for automatic mapping of shaded ice in bright zones. Correct glacier boundaries were indicated manually at the difference between them (regardless of the debris-covered ice), which generally cover blue boundaries in (a) and yellow boundaries in (b), respectively.

https://doi.org/10.1017/aog.2023.75 Published online by Cambridge University Press

the timestamp of the interference pair, which is a judgmental process. In some cases, when preliminary estimates of glacier extent are made from glaciological relationships, a tiny accumulation area may not yield a large glacial tongue (Molg and others, 2018). Moreover, reexamining previous inventories and their source images can provide important references.

Rock glaciers are typically permafrost creep features with high debris content, moving downslope by a few centimeters to a few meters per year, and may originate from ice-cored moraines or be located on talus slopes that provide a continuous debris input (Haeberli and others, 2006; Berthling, 2011; Monnier and Kinnard, 2015; Molg and others, 2018). However, the investigation of rock glaciers in Antarctica and Greenland is inadequate and limited to small regions (Rudolph and others, 2018; Abermann and Langley, 2022) and previous inventories do not provide any information on the separation of rock glaciers from glaciers. It is difficult and highly subjective to distinguish rock glaciers from similar features, such as debris-covered glaciers and ice-cored moraines in 30 m spatial resolution images or even in high-resolution images (Janke and others, 2015; Paul and others, 2017; Reinosch and others, 2021). Line-of-sight (LOS) surface velocity estimation from InSAR has been applied successfully to determine rock glacier activity in regional inventories in recent years (Villarroel and others, 2018; Strozzi and others, 2020; Brencher and others, 2021; Reinosch and others, 2021; Zhang and others, 2021). However, InSAR suffers from limitations closely related to rock glacier studies, including underestimation of true 3D velocities, decorrelation arising from changing surface properties, atmospheric delay and the maximum detectable displacement between two SAR acquisitions (Villarroel and others, 2018; Brencher and others, 2021; Reinosch and others, 2021). Mitigating these problems requires careful study designs and a considerable amount of work. In addition, it remains difficult to define indicators to distinguish rock glaciers from debris-covered glaciers because they may have similar rates of movement (Villarroel and others, 2018). Unlike debris-covered glaciers with longitudinally flowing ridges and distinct lateral and central moraines, rock glaciers tend to exhibit pronounced transverse ridges and furrows perpendicular to flow direction, showing lobate (width-to-length ratio ≥ 1) or tongue-shaped (width-to-length ratio <1) forms (Janke and others, 2015; Tanarro and others, 2018; Strozzi and others, 2020). Therefore, we excluded rock glaciers by using high-resolution images to identify landforms and the morphology of debris accumulation on the glacier surface. When high-resolution images are missing and difficult to judge, we relied on coherence images for mapping because it helps to exclude at least inactive rock glaciers, but may result in an overestimation of debris cover.

3.2 Delineation of glacier divides

The next step in creating a glacier inventory is to separate glacier complexes based on hydrologic divisions, and the location of the divides determines the number and area of individual glaciers (Paul and others, 2002; Ke and others, 2016). Racoviteanu and others (2009) recommended that ice divides should be placed in the same location as in previous inventories when comparing glacier extents. However, previous inventories used early DEMs as input for watershed analysis, and their vertical accuracy and resolution is inadequate compared to recently published DEMs (see section 2.3). Inaccurate and coarse DEMs can lead to topographic divisions that differ from the true topographic divides, ultimately resulting in shifted glacier divides (Kienholz and others, 2013).

We referred to the semi-automatic method of Bolch and others (2010) and Kienholz and others (2013) to create buffer zones around each glacier complex. This method can be used for any time period and extent (Bolch and others, 2010) and is very conducive to splitting glaciers with significant topographic variation in the accumulation zone (e.g. protruding rock ridges or summits). We clipped the DEM to the buffer zones and calculated the glacier basins using watershed analysis tools in ArcGIS. Basins were created automatically by locating pour points and depressions at the edges and determining the convergence area of each pour point. We subsequently converted the calculated basin raster into polygons representing the glacier basins. These polygons were merged to clip the glacier complexes supported by aspect and ice velocity maps, and with reference to the merging rules of the previous inventories. However, potential DEM artifacts in the accumulation zone can lead to errors in the automatically derived ice divisions (e.g. Bolch and others, 2010; Ke and others, 2016) and significant uncertainty in demarcating glaciers in areas of flat accumulation that lack distinct topographic features to support visual judgments. Therefore, we manually corrected the watershed by combining color-coded flow-direction grids in the background (e.g. Paul and others, 2011), hillshade maps, optical scenes and ice velocity maps to reduce the error. Finally, sliver polygons created by the intersection of watersheds with glacier boundaries due to the possible differences between the DEM used for the orthorectification of the optical image and the DEM used to derive ice divides were checked and manually corrected.

Separating glaciers among ice fields is quite challenging in the study area. A large outlet glacier may originate from numerous interconnected valley glaciers or the ice sheet upstream, which increases the difficulty of assigning glacier extent. The divisions used in the previous inventories were useful in reducing the effort to trace accumulation areas of the glacier. Importantly, we checked and adjusted the extent of individual glaciers based on the ice velocity map. As in the previous inventory, to divide a very large glacier in intricate terrain, some glacier divisions were added even though they lack support information.

In Greenland, the watersheds generated by Rastner and others (2012) based on the GIMP DEM were used not only to define glacier divisions, but also as connections between the GIC and the ice sheet, with CLs defined as weak (CL1) and strong (CL2). Here, another challenge occurred: the position of these boundaries changed when the watersheds were generated from a new DEM, either considering real topographic variations or the effect of different vertical accuracy and resolution of the DEM. Secondly, the separation of the GIC from the ice sheet in the previous inventory is necessary, while the merging of basin polygons and glacier divisions here can be very subjective and straightforward (accumulation areas that contribute to glacier flow may not be included in the GIC). Therefore, we decided to retain the watersheds generated by Rastner and others (2012) using GIMP DEM where glaciers are connected to the ice sheet and use new watersheds to divide the glacier complexes. The reasons for this are: (1) RGI 6.0 has been used in many existing studies; (2) the difference in watersheds derived from the GIMP DEM and the ArcticDEM is acceptable (see section 5.3); (3) the inconsistency in glacier definition due to artificial factors and differences in accuracy of DEM can be avoided; (4) this provides advantages in time series analysis of glacier change; and (5) glacier area generally changes very little at the internal basin boundaries with the ice sheet even when surface elevation changes.

3.3 Assignment of glacier attributes

To complete the glacier inventory, the necessary fields such as source date, glacier area, minimum, maximum, median and mean elevations, mean slope and aspect, and CLs were created for each glacier outline. For the same glacier mapped with

https://doi.org/10.1017/aog.2023.75 Published online by Cambridge University Press

multiple images, the last acquisition date of the images was taken as the as-of-time (i.e. source date; GLIMS Analysis Tutorial, https://www.glims.org/MapsAndDocs/guides.html). In this work, glacier areas were calculated using the South/North Pole Lambert Azimuthal Equal Area coordinate system. Attributes of glacier-specific topographic parameters (e.g. elevation, slope and aspect) were calculated by combining the glacier outlines with the topographic raster using the zonal statistics tool in ArcGIS. This tool statistically summarizes the values of the topographic raster dataset within the glacier outline zone and links the results to the glacier outline attribute table using a common and unique identifier (i.e. the glacier ID).

In Greenland, glaciers classified as CL0 have no connection with any other class, CL2 glacier complexes have a relatively stable boundary in contact with the ice sheet and CL1 glacier complexes may have contact with the ice sheet in the accumulation or ablation zones. Glaciers in contact with the ice sheet are assigned CLs first. Due to the 'topological heritage' rule, the connected entities (in the glacier complex) of glaciers that have been assigned CLs also adopt the same class (see Rastner and others, 2012), so that the CLs of a set of entities can be co-varying. However, changes of individual glaciers are difficult to describe systematically, for example: some local glaciers may have disappeared and individual glaciers may have changed due to glacier division shifts; glaciers that were originally part of a glacier complex may have separated due to ablation, especially where the topography is prominent and originally divided by a watershed; and glacier tongues that retreated in the ablation zone lost contact with the ice sheet. All of these may lead to a change in CLs of glaciers with the ice sheet from high to low. Therefore, we emphasize that the CLs of Greenland glaciers need to be checked again.

4. Application and results

In this section, we present and discuss the application and results of updating glacier outlines in representative areas of Antarctica and Greenland following our approach outlined in the methods. We take James Ross Island (this case gives glacier attribute samples; Table 1), Ross Island and the region around Kangerlussuaq Fjord as application cases (Fig. 1). The updated glacier outlines were overlaid on the background images and compared qualitatively with the previous inventories. Watersheds are difficult to compare because they are affected by the date (thus need to take into account glacier and terrain changes) and accuracy of the DEM (Kienholz and others, 2013). In addition, the rules for merging basins are not always consistent due to different processing procedures. The ability of watersheds generated from DEMs of different periods to reflect the true glacial topographic divisions during the corresponding periods in areas of weak glacial and topographic variability is discussed in section 5.3 with examples.

Due to the lack of ground truthing, we quantitatively assessed the uncertainty or precision of the updated glacier outlines, rather than the accuracy (Paul and others, 2017; Molg and others, 2018). For glacier boundaries, the uncertainty or precision is determined in two different ways: in the case of automatically derived boundaries, values were taken from the literature or manual digitization results based on the same images were compared; in the case of manually digitized or improved boundaries, the results of mapping based on higher-resolution images are used for cross-validation. However, problems with high-resolution imagery in Google Earth, including different source date, small spatial coverage, potential snow, cloud and shadow conditions, and the quality of DEM used for orthorectification, limit its ability to be used as reference data (Paul and others, 2017). We mitigated these influences by selecting high-resolution images with close timing to the used Landsat images and better mapping conditions (e.g. less cloud and snow cover) and geographic registration accuracy. We also assessed the precision of glacier divides based on light and dark divisions in the background images or by comparison with the results of visual interpretation at clear topographic divides.

4.1 Case study 1: James Ross Island

Glaciers on James Ross Island terminate on land or in the ocean, and can be covered in debris that is uncommon in other parts of Antarctica. These glaciers are considered to be ice caps and not divided by watersheds (Bliss and others, 2013).

The OLI8/OLI6 ratio image (L1) includes more shaded ice in dark zones at a threshold of 1.51 and a higher threshold of 1.85 was applied for brighter bare rock and shadows (Fig. 5a). We cropped ratio images to a buffer (1 km) of the REMA contour at the edges of the island (25 m) to reduce the processing efforts and manually corrected the automatically derived boundaries (Figs 5b, c). Raw and threshold coherence images and optical images were used together to reduce the selection omission of ice pixels. Using multi-time images (1988, 2000, 2015 and 2021) and high-resolution images in Google Earth, land cover types such as snow and debris cover were discriminated and mapping challenges were addressed. We primarily used the C1 coherence image and the optical images near the time of interference pairs to exclude coherence loss which probably occurred due to snowfall and melting (Figs 5d, e). Possible snow or ice cover that matches the irregular shape features and shows higher coherence (>0.4) was regarded as snow and excluded. The decision process was also supported by a combination of five additional coherence maps (C2–C6) with different time baselines and the previous inventory.

The overlay of outlines shows the corrections to the automatically derived glacier outlines (Figs 5b, c), and explains the differences with the previous inventory (Figs 5f, g). Some differences were carefully examined in high-resolution images from Google Earth and did not create ambiguities. Previous and updated glacier outlines are able to correctly represent most of the clean ice from the corresponding period. However, excluding factors of

Table 1. Attribute examples of CL0 glaciers (1–9 in Fig. 6) with source date of 23 Dec 2021 and deviations between Landsat and Google Earth results

Glacier ID	1	2	3	4	5	6	7	8	9
Minimum elevation (m)	72	21	21	22	21	22	21	74	23
Mean elevation (m)	191	139	303	285	165	131	88	118	166
Median elevation (m)	184	125	375	331	151	120	80	109	177
Maximum elevation (m)	358	369	448	466	440	318	229	209	352
Mean slope (°)	16	13	10	12	12	22	23	22	8
Mean aspect (°; clockwise from North)	110	97	145	138	239	77	266	274	248
Landsat area (km^2)	0.3969	1.3078	7.9065	6.8352	3.8490	0.6560	0.2524	0.1119	4.7213
Google Earth area (km^2)	0.3896	1.3153	7.7559	6.7398	3.7296	0.6764	0.2537	0.1347	4.9386
Area deviations of Landsat and Google Earth	1.83%	0.57%	1.92%	1.41%	3.15%	3.06%	0.50%	18.44%	4.50%
Distance deviations of Landsat and Google Earth (m)	32		27			23	40	16	38

https://doi.org/10.1017/aog.2023.75 Published online by Cambridge University Press

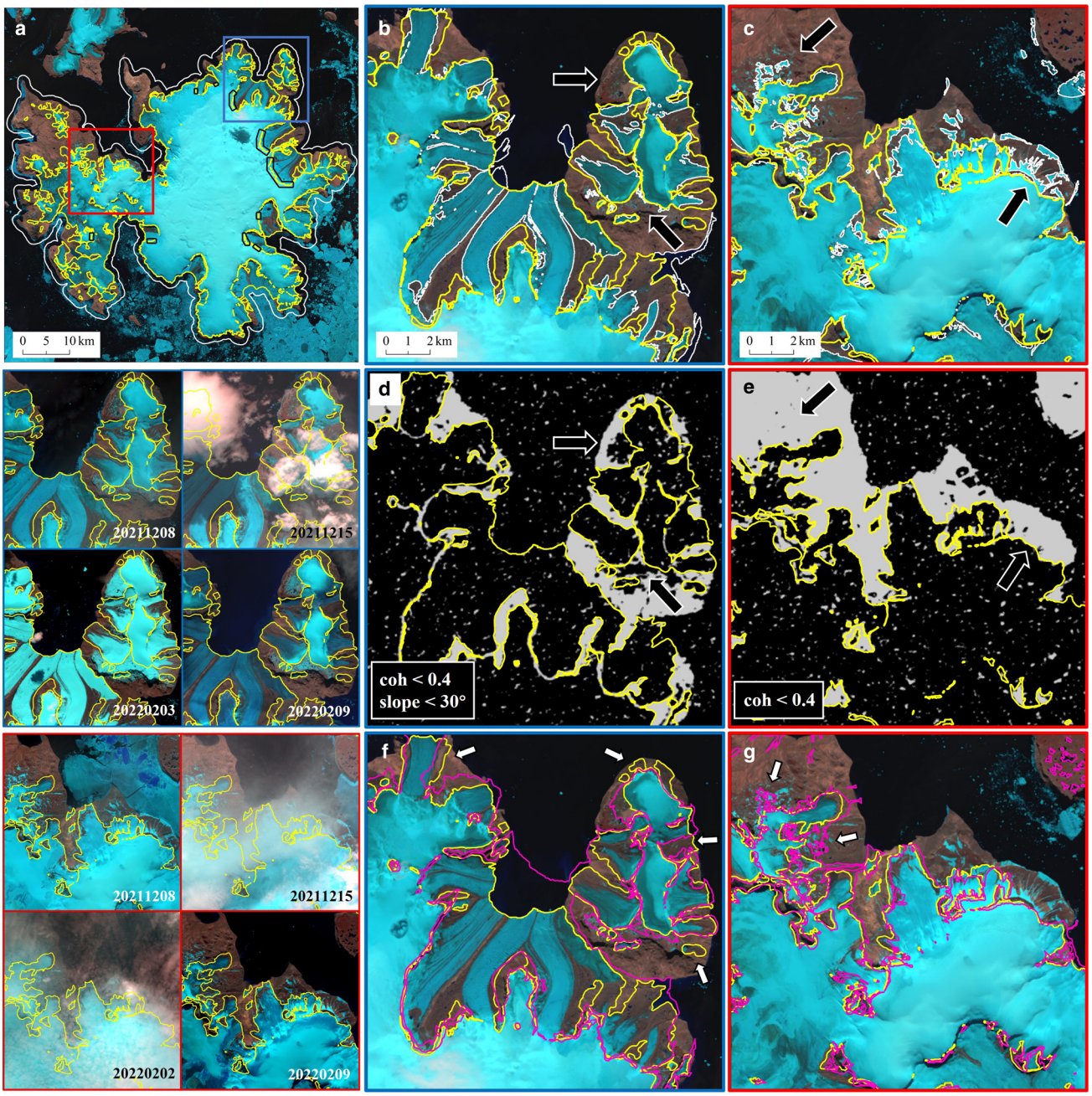

Figure 5. Application case of the methods for James Ross Island in AP. (a) Glacier scene (L1, 20211223) with updated glacier outlines (yellow). The blue and red boxes correspond to the scene subsets (b, d, f) and (c, e, g), respectively. White represents the buffer (1 km) zone of the REMA contour (25 m). A higher OLI8/OLI6 ratio threshold (1.85) was used within the created masks (black). (b, c) Selected examples of the correction to the raw classification results (white). (d, e) The use of threshold coherence map (C1, 20211212-20220204; a 3 × 3 low-pass filter was applied to smooth boundaries) to support glacier mapping. The left insets provide a further view of the optical images near the time of interference pairs for the blue and red boxes in (a). The black arrows in (b, d) indicate that coherence loss due to snowfall is excluded when plotting glaciers and in (c, e) indicate that the exclusion of snow or ice cover that matches the snowpack features and shows higher coherence. (f, g) Comparison of updated glacier outlines with RGI 6.0 (purple). The white arrows indicate where the updated glacier outlines and RGI 6.0 differ in terms of debris and snow cover.

glacier variability and outline positioning accuracy creates large differences in the interpretation of debris and snow cover. From the assessment factors of the Third Pole inventories by He and Zhou (2022), the medium- to high-resolution scenes, unstriped imagery and less snow and shadows, as well as the combination with InSAR technique, are favorable to reduce uncertainty in the process of updating glacier outlines here.

Automatic mapping of clean glaciers is at least as accurate as manual digitization, or has only single-pixel differences (Paul and others, 2013). As shown in Figure 6, we depicted nine debris-covered glaciers based on high-resolution images in Google Earth with close timing to a Landsat image (L1, 20211223) and calculated their area deviations. The calculated area deviation value in Table 1 tends to increase toward larger glaciers (e.g. Paul and others, 2013, 2017), so it is inappropriate to apply these percentages for the entire glacier area. As in many studies (e.g. Granshaw and Fountain, 2006; Bolch and others, 2010; Rastner and others, 2012), the glacier buffer approach was used to calculate the relative change and estimate the uncertainty in glacier size. The mapping results from Google Earth were converted from KML to SHP, which can be loaded into ArcGIS and then compared with Landsat boundaries. Points were taken every 30 m along the Landsat boundary and their distance from the nearest points on the corresponding Google Earth boundary

https://doi.org/10.1017/aog.2023.75 Published online by Cambridge University Press

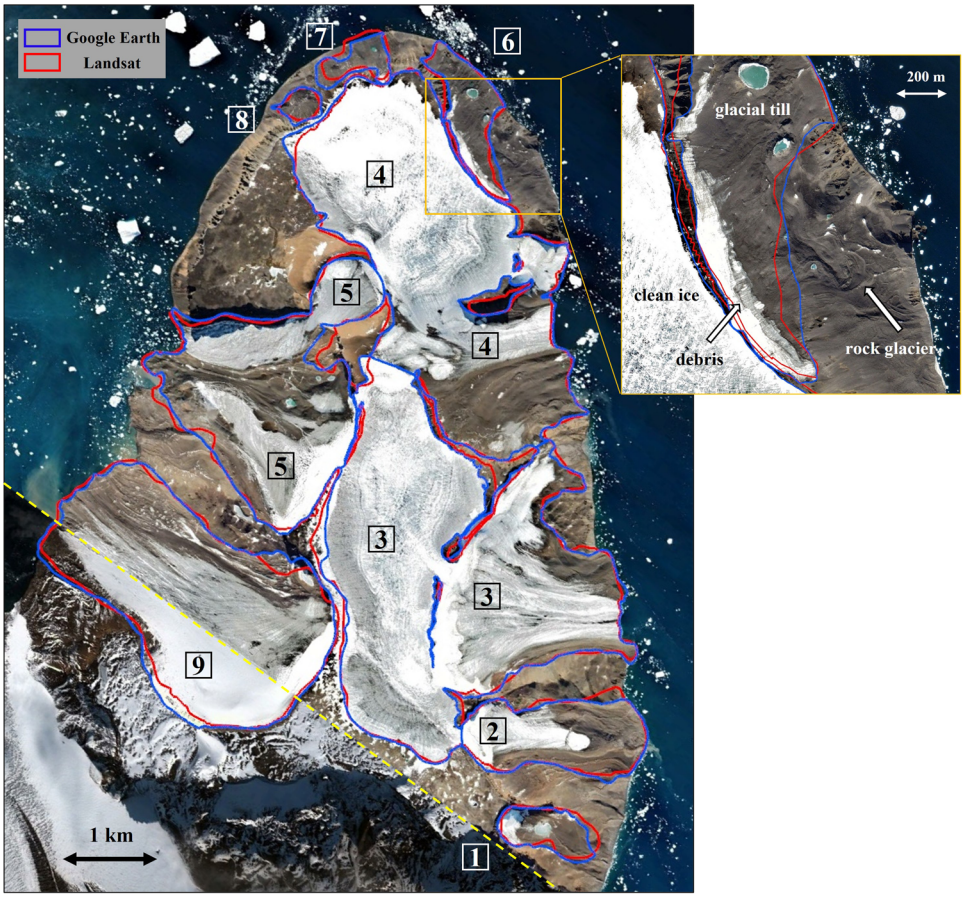

Figure 6. Overlay of boundaries of nine glaciers (1–9) on James Ross Island mapped using Google Earth and Landsat, with a high-resolution screenshot from Google Earth. The upper scene (17 Jan 2021) and the small scene below (18 Mar 2009) are separated by the yellow dash line. The center glacier complex was divided based on 3D views in Google Earth to facilitate comparison of glacier areas. The right inset shows an ice-debris landform and the features of the moraine deposits here are consistent with ice-cored moraine characteristics described by Strelin and Sone (1998) and buried glaciers described by Janke and others (2015), including appearance of pockmarks, ponds and weak development of surface ridges. Please note the coherence information at the corresponding location on the right side in Figure 5d. It is difficult to accurately separate rock glaciers even in Google Earth because they have obscure transitions with debris-covered glaciers.

was calculated (this method is referred to as the nearest neighbor method in the following sections; e.g. Guo and others, 2015). Glaciers have an average distance deviation of about 1 pixel or 30 m between the two boundaries (Table 1). Applying this deviation to the buffer method, we obtained an uncertainty of 2.4% in the mapped glacier area of James Ross Island.

4.2 Case study 2: Ross Island

The majority of the glaciers containing glacier watersheds on Ross Island are marine-terminating, either with ice shelves or connected to sea ice at the margin, and a small number are land-terminating.

Three images from 2018 (L2–L4) with various enhancements served as inputs for mapping the glacier boundaries. REMA was used to generate contours for providing a reference for image-based manual digitization of glacier boundaries (Figs 7b, c) and create watersheds following the method described (Figs 7g–i). In most cases, the land-terminating glacier boundaries were not mapped manually, but were obtained by excluding rock outcrops within the mapped outer boundary (i.e. the outermost edges of the island are regarded as the glacier outer boundary; Figs 7d–f). The raw images (L2) were processed in ENVI to obtain TOA reflectance corrected and brightness-temperature converted data. The glacier outer boundary mask and a set of thresholds were used to produce the rock outcrop raster (NDSI >0.7, blue <0.32 (a single blue threshold is sufficient to map this scene with more consistent shading conditions), TIRS1/blue >400, TIRS1 >255 K). Six coherence images (C7–C12) with a stack of their minimum values and additional Landsat scenes (2001, 2014 and 2019) were used to view snow conditions and support the modification of snow-covered rock areas (Fig. 7e). The rock outcrop vectors were intersected with the glacier outer boundary and watersheds to derive outlines of Ross Island glaciers (Fig. 7a).

When updated glacier boundaries and those in RGI 6.0 were overlaid for comparison, significant positioning and generalization differences can be observed (Figs 7b, c, f). Actually, glacier boundaries in the previous inventory by Bliss and others (2013) were derived primarily from polygon files from ADD 3.0, which were manually created based on sources with various resolutions and accuracies (e.g. paper maps, aerial photographs and optical images). The previous rock dataset has some significant georeferencing inconsistencies, misclassifications and overestimation of Antarctic ice-free areas (Burton-Johnson and others, 2016). Therefore, the accuracy of this inventory is regionally inconsistent and without associated quality assessment. In our work, the original data sources are from the Landsat L1 T dataset (see section 2.1), which includes accurate geographic calibration and orthorectification using digital topography (Wulder and others, 2012). As a result, the updated glacier boundary is of high global positioning accuracy. We used elevation references from REMA in addition to planimetric imagery to reduce the subjectivity of mapping glacier boundaries. The classification accuracy of Burton-Johnson and others (2016) method for rock pixels is 74 ± 9% and is more

https://doi.org/10.1017/aog.2023.75 Published online by Cambridge University Press

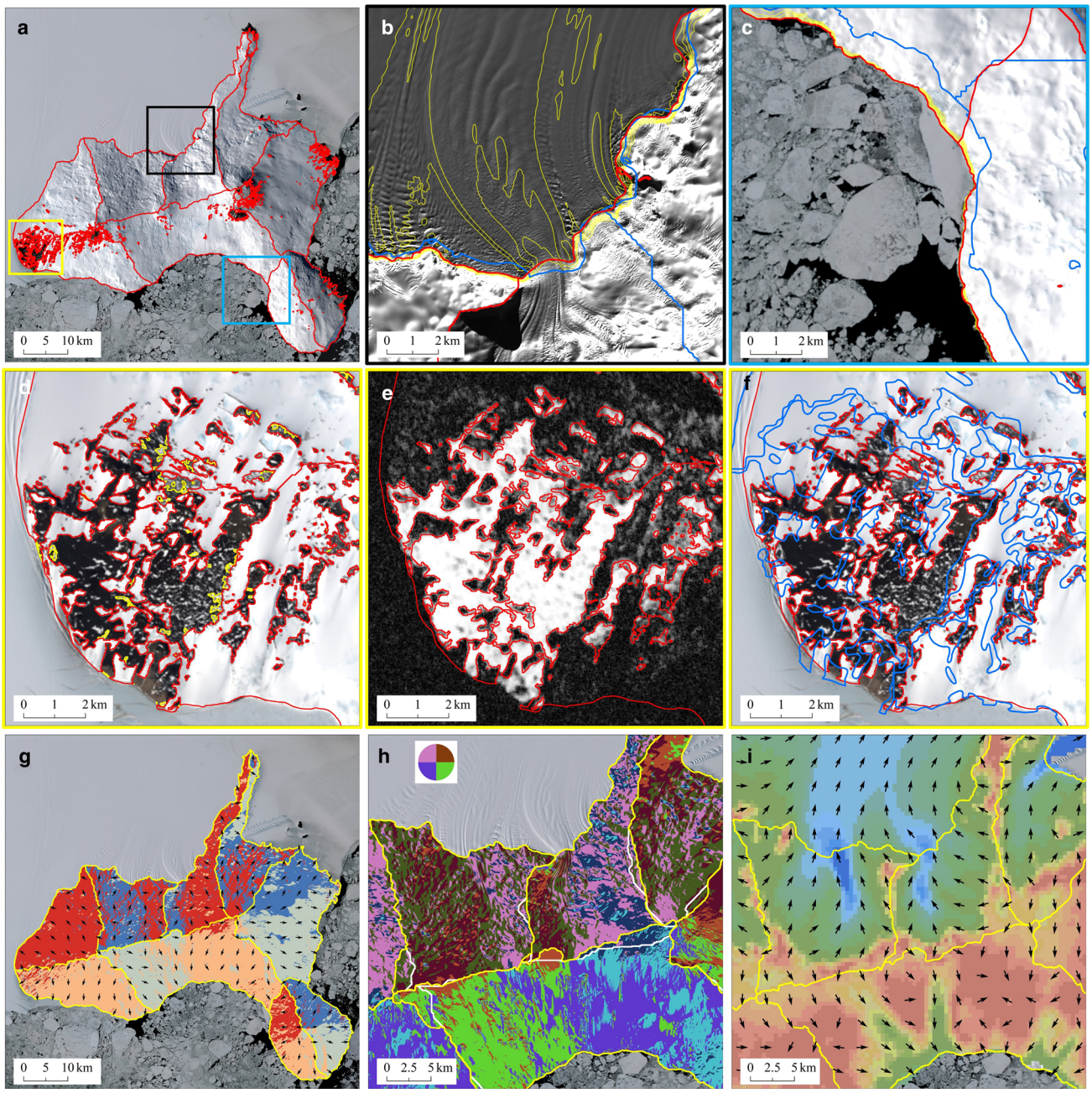

Figure 7. Application case of the methods for Ross Island in EA. (a) Glacier scene with updated glacier outlines (red). The black, blue and yellow boxes, respectively, correspond to the scene subsets (b, c) and (d, e, f). (b, c) Selected examples of ice-shelf-terminating and marine-terminating outer boundary mapping, respectively, with (enhanced) images and contours (yellow; −30, −15, 0, 15, 30 m) generated from REMA. Glacier outlines from RGI 6.0 are shown in blue. (d) Selected example of the correction to the raw rock classification results (yellow) at the snow cover. (e) Minimal composite from six coherence images (C7–C12) helps exclude blurred snow patches around glaciers. Dark color indicates areas of low coherence. (f) Comparison of updated glacier outlines with RGI 6.0 in rock area. (g) The intersection (yellow) of glacier outer boundary and watersheds with an aspect map. (h) Correction to the raw watersheds (white) with the help of the color-coded flow-direction grid. (i) Direction and magnitude (blue>green>brown) of ice velocity guide the delineation of glacier divides.

accurate and consistent than the ADD rock dataset (only 39 ± 19%) (see Burton-Johnson and others, 2016), so the improvement in rock classification accuracy is significant.

We used Google Earth with the excellent 3D rendering and high-resolution images to help assess the precision of manually mapped glacier outer boundaries. In the mapping process, the image at 30 m resolution (Dec 2018) was used as the primary reference. In areas with less intense glacier variability, images with a resolution of less than 1 m from different years (2011, 2012, 2015, 2017 and 2021) were also referenced to provide a finer representation of the boundaries (Fig. 8a). The glacier boundary, which was drawn based on images from different years, was checked for matches with the Dec 2018 image and adjustments were made. The 3D terrain height display in Google Earth was expanded threefold to better visually represent the boundary between glacier and ice shelves (Fig. 8b). We used the nearest neighbor method to calculate the deviation from the Google Earth boundary for every 100 m of sampling points on the Landsat boundary (Fig. 8c). The results show that the overall average deviation is about 32 m, the average deviation of the boundary between glaciers and ice shelves (including the glacier outlet) is about 58 m, and for the boundary between glaciers (or island) and the ocean (including very few land-terminating boundaries) the average deviation is about 20 m. Most of the deviations above 90 m occur at the glacier outlet and the boundary between glaciers and ice shelves. The difference in area enclosed by the two

https://doi.org/10.1017/aog.2023.75 Published online by Cambridge University Press

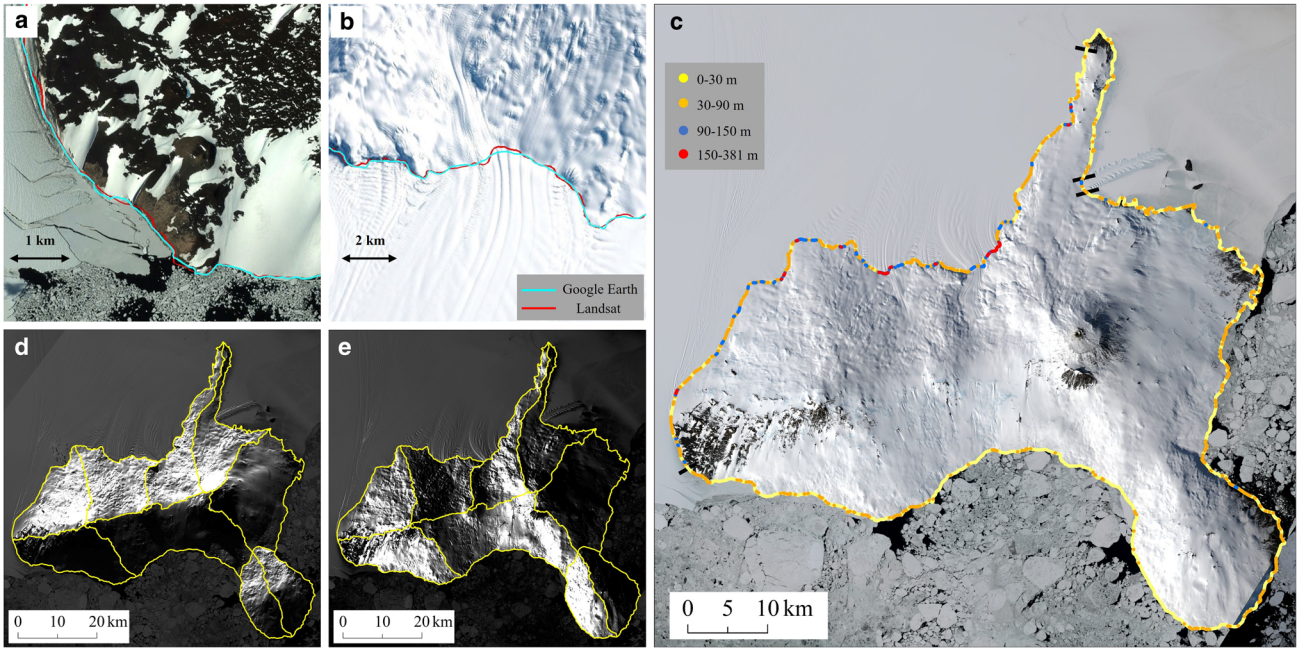

Figure 8. Precision assessment of glacier outlines on Ross Island. (a, b) Two examples of precision assessment of glacier outer boundaries on Ross Island. Blue indicates boundary mapping using high-resolution image (30 Dec 2011) and using 3D view (Dec 2018) from Google Earth, respectively. Red represents the boundary mapped based on Landsat images. (c) Deviations between Landsat and Google Earth boundaries. The black truncated lines indicate the boundary division of ice shelf terminus and ocean terminus. (d) (e) The intersection of glacier outer boundary and watersheds and two stretched images (L2, L3) with sun azimuths near perpendicular to each other.

sets of glacier boundaries was calculated, and the results show that the area derived using Google Earth is approximately 0.11% larger than that derived from Landsat images using our approach.

We used a method that considers the length of the glacier boundary and its positioning accuracy to assess the total area error of glaciers on Ross Island (Rivera and others, 2005; Guo and others, 2015). The evaluation of the glacier area error is calculated from the following equation:

$$E_A = L_1 D_1 + L_2 D_2 + 0.26 A_R \quad (1)$$

where E_A is the glacier area error, L_1, D_1, and L_2, D_2 are the length and average deviation of ice-shelf-terminating and marine-terminating glacier boundary, respectively, and A_R is the total area of rock outcrops, obtained by subtracting the area of final glacier outlines from the area of the outer glacier boundary. The rock classification accuracy was considered to be 74% and the value of 0.26 was used as the factor for the rock area error term. Manual corrections were made to the automatically derived rock classification results, so this is an upper bound estimate. It is shown that the glacier area error contributed by the glacier outer boundary is 0.44% and by the total rock area is 1.14%, so the total area error is 1.58%.

The watersheds generated using REMA perform well and the stretched images were used as background for examining the watersheds. As shown in Figures 8d, e, the watersheds are able to match the light and dark divisions in the stretched images well. Visual checks of watersheds at clear topographic divisions in the image show average deviations that are about one pixel (32 m).

4.3 Case study 3: Kangerlussuaq Fjord

The study area with GIC of all CLs around Kangerlussuaq Fjord has different local lighting conditions due to the complex terrain and contains clean or dirty ice, shaded ice and more debris-covered ice.

Three median-filtered OLI8/OLI6 ratio images of the same OLI scene (L5) were cropped and mosaicked to map glaciers with varying local illumination conditions in this region: an OLI8/OLI6 threshold of 1.75 was used for bright snowfields on high terrain, and low thresholds of 1.35 and 1.50 were used to map dark zone glaciers on low-lying terrain near the coast (Fig. 9a). Boundaries between GIC and the ice sheet from the previous inventory were retained (Figs 9b, c) and misclassified boundaries were manually improved (Figs 9d–f). To address the challenges of snow, debris cover and shadows in this scene, another image from a close time (L6) was used and multi-temporal images (2000, 2002 and 2019) were viewed alternately. Two of the better coherence images (C13–C14) were used as the primary references and the rest (C15–C18) were used as supplementary references. The low consistency due to steep slopes in this complex terrain reduces the usability of raw coherence maps, so slope thresholds were selected and applied. We then used the ArcticDEM and watershed analysis tools to create the watersheds, modified and added some necessary divisions based on the flow-direction raster, optical images and ice velocity map (Figs 9g–i).

Glacier boundaries mapped by OLI are presented at a higher resolution, so more details are mapped that better reflect the condition and extent of the glacier. Section 5.2 compares the differences in glacier mapping results using OLI and ETM+ at different resolutions. We combined the advantages of mapping shaded ice by OLI with the multi-threshold method to obtain the ice classification results for locally different illumination conditions in a single scene without compromising on threshold selection. As a result, most of the clean and shaded ice in the scene is automatically and accurately drawn, even if they are in areas of different brightness. In particular, few manual improvements are required for rock outcrops mapped in scenes with little seasonal snow, which is useful for mapping glacier outlines containing large amounts of rock outcrops in Greenland.

The precision of glacier boundaries is usually determined by the threshold value for the image ratio and the key is whether the threshold can be satisfied for most areas of the scene, even

https://doi.org/10.1017/aog.2023.75 Published online by Cambridge University Press

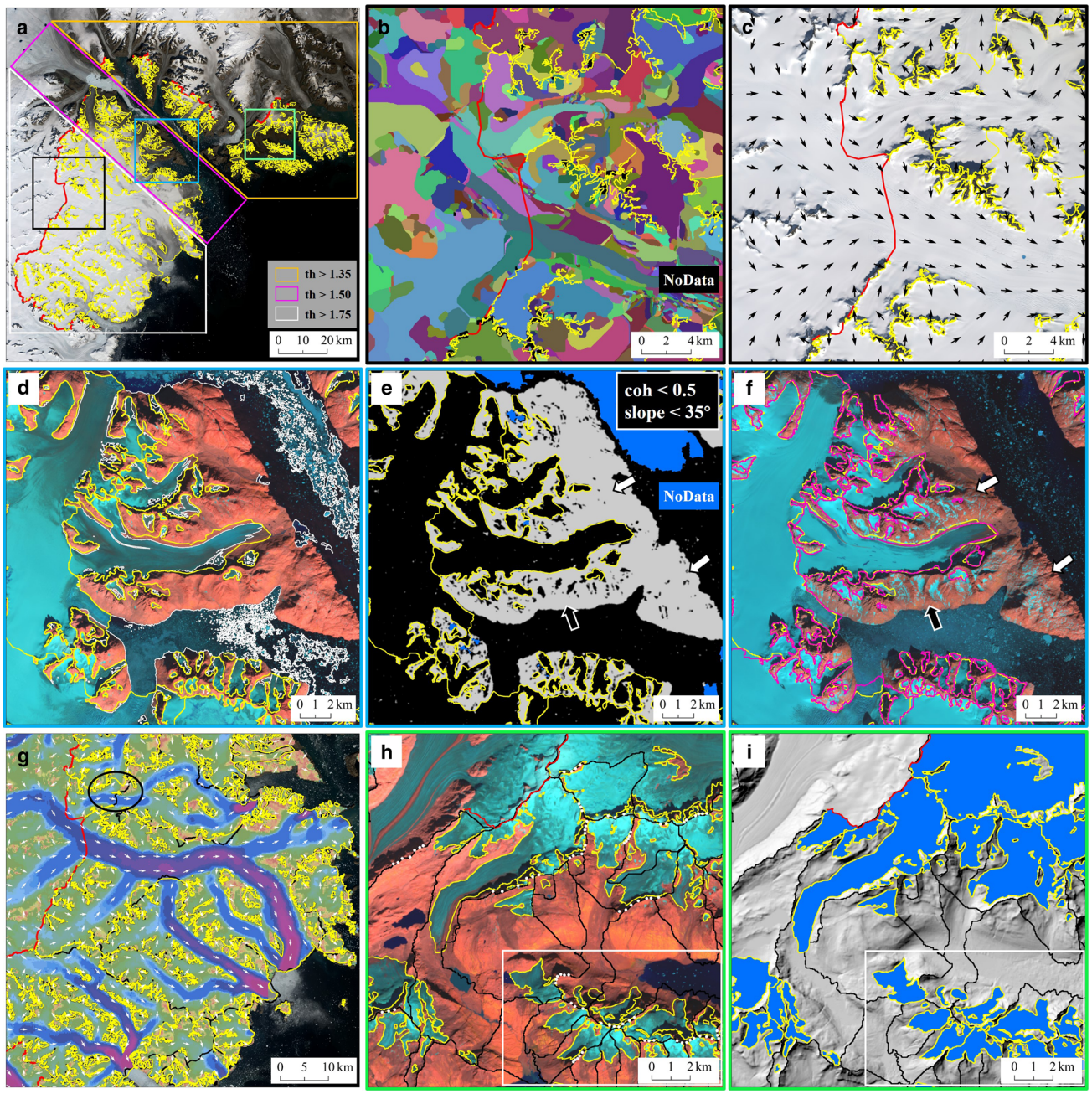

Figure 9. Application case of the methods for the region around Kangerlussuaq Fjord in CE Greenland. (a) Different OLI8/OLI6 thresholds were used for the glacier scene (L5, 20140816) to update glacier outlines (yellow), preserving boundaries between GIC and ice sheet from RGI 6.0 (red). The black, blue and green boxes correspond to the scene subsets (b, c), (d, e, f) and (h, i), respectively. (b, c) respectively, explain that the basin raster and the direction of ice flow may not support the demarcation of GIC and ice sheet, which is influenced by artificial factors. (d, e) An example of correction to the raw classification results (white) guided by the optical scene and the threshold coherence map (C14, 20150813–20150906), respectively. (f) Overlay of updated and RGI 6.0 (purple) glacier outlines on the glacier scene (20150828). In (e) and (f), the interference of low coherence due to snow melting at the black arrow was excluded and some snow patches at the white arrows were filtered by the coherence threshold. (g) Dividing glaciers on an intricate ice field with the help of the magnitude (purple>blue>green>brown) and direction of ice velocity. The watershed in the black circle aims to divide a very large glacier, but lacks information to support it. Black are outlines of the overlaid RGI 6.0. (h) The raw merged basin polygons (black), with manually identified dots (white) on the watershed. (i) Final divided glacier extent (blue) in (h), with a hillshade map. The accumulation areas of some glaciers are already separated by ridges without help from watersheds (white boxes in (h, i)).

if some areas (e.g. deep shadows, clouds and debris cover) must be manually improved. A rock outcrop and two representative clean (or slightly dirty) glaciers, which respectively represent the classification results for shaded ice in the brighter zones, ice in sufficient light and shaded ice in dark zones, were manually digitized to compare with the automatic results using the nearest neighbor method (sampling point interval of 10 m on the automatic boundary) and test the applicability of different thresholds to this scene (Figs S1a–S1c). We also depicted three debris-covered glaciers based on images with close timing (26 Jul 2012) in Google Earth and calculated their deviations from the manual Landsat mapping results using the same method (sampling point interval of 10 m on the Landsat boundary; Figs S1d–S1f). Therefore, we used a 15 m buffer around all glacier complexes based on the average of the deviations in Figure S1, and thus calculated the uncertainty of 2.7% for the updated glacier area around Kangerlussuaq Fjord.

The precision of watersheds derived from ArcticDEM was evaluated. With the help of images and Google Earth, we visually identified 90 checkpoints on distinct topographic divides where

https://doi.org/10.1017/aog.2023.75 Published online by Cambridge University Press

automatic basin polygon boundaries matched the flow-direction divisions to compare with the raw merged basin polygons (Fig. 9h). The average deviation evaluated using the nearest neighbor method is about 24 m, which is within one pixel of the DEM (32 m).

5. Discussion

5.1 Effects of terminus types on mapped glacier area in Antarctica

In Antarctica, the manually digitized glacier boundaries can be quite long due to the influence of ice shelves and sea ice. The error in identifying glacier boundaries on images varies depending on the terminus type (e.g. Bindschadler and others, 2011). The accuracy of boundary mapping is critical for determining glacier area, while the uncertainty of glacier mapping needs to be additionally considered in change analysis. Based on the methodology of this study, we have attempted to assess the effects of terminus characteristics on manually mapped glacier area based on the significance of measured changes in glacier area.

Paul and others (2013) showed the results of their repeated experiments and suggested that glacier outlines should be digitized multiple times and that the average of the results from multiple digitizations is close to the true value. Seven ice caps without rock outcrops in EA and WA were selected (Fig. 10a), so the outer boundaries drawn represent their areas. We digitized their boundaries three times each independently and completed the experimental assessment based on the standard deviation (STD) of these results (Fig. 10). The land-terminating boundary has the same easily distinguishable characteristics as the marine-terminating boundary and thus is not considered. The length of coastline accounts for various proportions of each glacier boundary, and glaciers vary in size and are located in different regions. We then calculated the mean and STD of the triple results for each glacier and show them in Table 2.

The results show a maximum STD for glacier area of 0.41% and a minimum of 0.02%. The significance of the change in digitized glacier area does not appear to be related to the area of the digitized glaciers, but is somehow implicitly related to the nature of the boundary and closely related to how easy it is to interpret the glacier boundaries from the images. The area results from multiple measurements become more discrete when the length fraction of the boundaries connected to the ocean in the total boundary is reduced, and conversely it becomes more consistent. Line segments can often be traced to the nearest pixel when mapping glacier boundaries with the ocean (Fig. 10e), but the low contrast between glacier and ice shelf causes many difficulties in defining and identifying some glacier boundaries with ice shelves. In areas where it is difficult to interpret the glacier boundaries from the imagery, such as shaded areas (Fig. 10b), glacier outlets (Fig. 10h) and where glaciers drain gently into ice shelves (Fig. 10c), misinterpretation can easily occur, leading to large discrepancies. In addition, if the image does not have distinct features, the number of vertices used to digitize the boundary lines where glaciers are connected to ice shelves is reduced, which affects the degree of glacier generalization. The difficulty of interpretation is greatly reduced when the glacier boundary is the coastline, and the boundaries are nearly coincident in each digitization.

5.2 Mapping comparison of Landsat ETM+ and OLI in Greenland

In Greenland, we compare differences in glacier mapping results due to sensor differences in resolution and ratio bands (i.e. OLI8/OLI6, 15 m vs. ETM+3/ETM+5 and ETM+1, 30 m). It is challenging to select common scenarios in Greenland available for comparison at the time of ETM+ and OLI overlap. Ultimately, we chose a scene in the southeast (SE) region of Greenland that was from the summer (but more snow patches were present; Fig. S2a), and the OLI scene (L16, 20130825) was taken one day before the ETM+ scene (L15, 20130826). We chose appropriate thresholds for the OLI and ETM+ image ratios in each case (OLI8/OLI6 >1.43; ETM+3/ETM+5 >1.49 and ETM +1 >54), so that ice in sunlight and most shaded ice areas could be accurately mapped. The classification grid was then median filtered, and most patches of snow were removed based on a 0.05 km^2 area threshold.

We show the processed results in Figure S2b for qualitative comparison. Compared to the ETM+ method, the OLI ratio produces glacier polygons that contain more detailed holes because the finer resolution allows more rock outcrops, contaminated ice and debris-covered ice to be separated from the ice classification results rather than being included in the mixed pixels. In addition, ETM+ images often contain snow patches or ice at the glacier boundary due to their coarse resolution, while OLI is able to detect the gap between the glacier and snow or ice, thus separating them.

The quantitative comparison of the two results is challenging and is very rule dependent, as there are few original glacier polygons that can be directly compared and manual corrections would introduce the same glacier area corrections. 84 glaciers (including snow) were separated from the raw automatically derived polygons in the common area (Fig. S2a). As in Figure S2, aiming to minimize the generalization differences between ETM+ and OLI, these glaciers were preprocessed under the principle of minimal manual intervention. The results show that the 84 glaciers from ETM+ have a total area of 207.8 km^2, which is 6.15 km^2 (about 3.1%) larger than the OLI result of 201.65 km^2. We show the relative area differences between these glaciers in a scatter plot (Fig. S3). The results show that the area of glaciers mapped by OLI is systematically smaller than that of ETM+. The relative standard deviation decreases and tends to stabilize with increasing glacier area.

5.3 Ice divide determination from watershed analysis tools

Here, we compare the differences in ice division using the previous DEMs (RAMP DEM, 200 m; GIMP DEM, 30 m) and the recent DEMs (REMA, 200 m; ArcticDEM, 32 m) in the study areas. We used the watershed analysis tools and the same basin merging rules to automatically generate watersheds from DEMs for selected glaciers (Fig. S4). At the same time, checkpoints were manually identified that visually matched the distinctly light and dark divisions and prominent ridges of the glacier scenes (L17–L22) from the early and recent periods, and were set only where the automatic basin polygon boundaries are consistent with the flow-direction grid divisions.

In Antarctica, the results show some large differences (Figs S4a, S4b). REMA watershed is in better agreement with the topographic divides shown in the contrast-enhanced images. We calculated an average deviation of about 107 m from the watershed of REMA and about 1743 m from the watershed of RAMP DEM by the nearest neighbor method. It should be noted that the difference in accuracy of DEMs is the dominant factor among the reasons for this difference over the entire period, and the difference in watersheds is relatively small due to temporal variation. The differences between ice divisions in Greenland are not significant: the GIMP-DEM watersheds and the ArcticDEM watersheds give deviations of 32 and 19 m, respectively (Figs S4c, S4d). Therefore, it can be demonstrated that the accuracy of watersheds generated using a high-precision DEM is improved when dividing glaciers in study areas with low variability of glacier and terrain.

https://doi.org/10.1017/aog.2023.75 Published online by Cambridge University Press

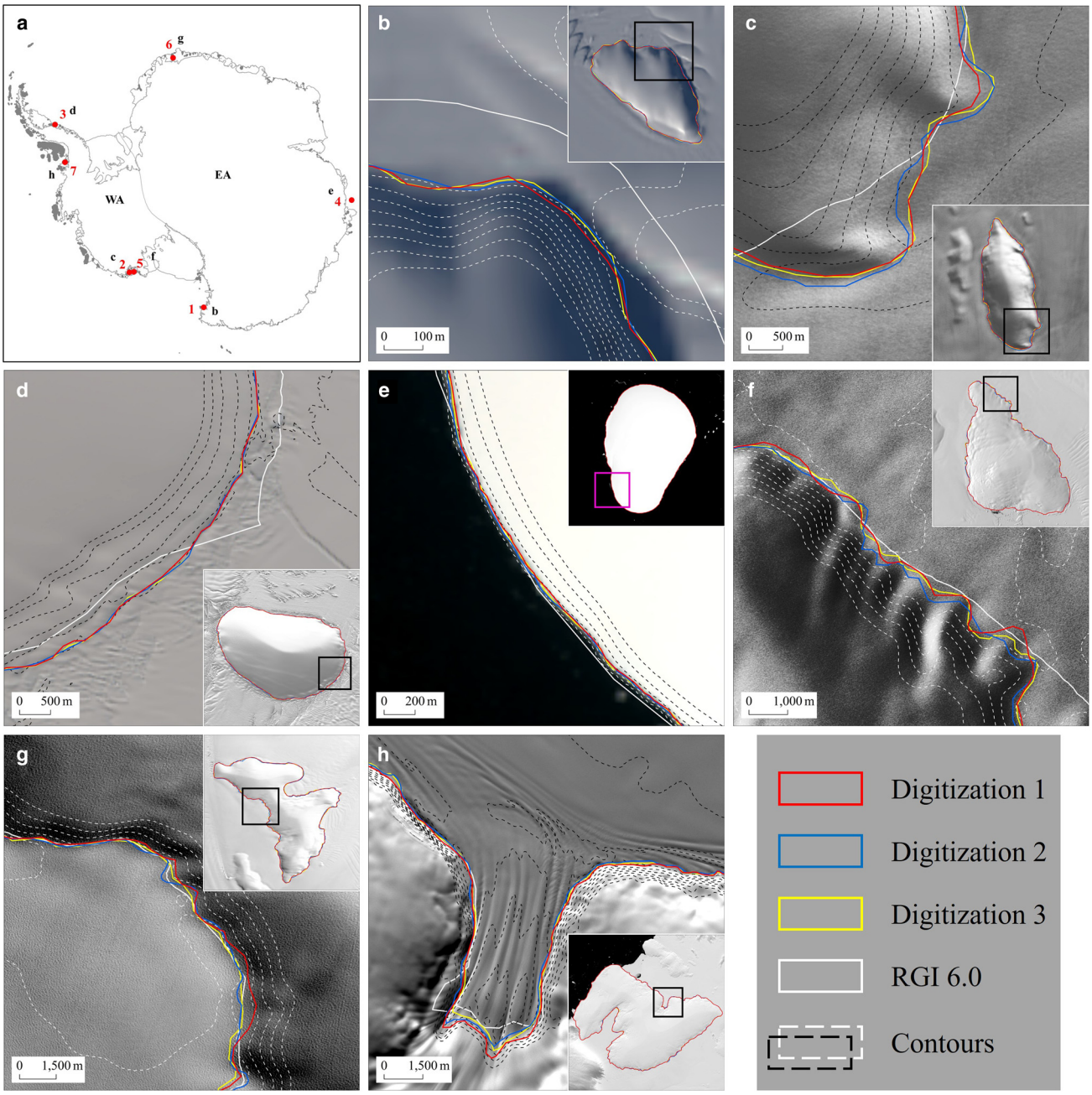

Figure 10. Assessing effects of terminus characteristics on mapped glacier areas in Antarctica. Seven glaciers have various sizes and locations, as well as different proportions of ice shelf and marine terminus (1–7 in (a) corresponds to (b)–(h)). Three separate digitizations were performed for each glacier. Contour lines with a contour distance of 10 m were generated from REMA.

5.4 Challenges and suggestions

The new source data and methods described in this study could be potentially used to update glacier inventories at a larger spatial scale in the study area and to evaluate the precision of glacier outlines. However, there are certain challenges in doing so, and we provide some suggestions here.

The main sources of uncertainty in glacier inventories can be positional errors (global control points), classification errors

Table 2. Results of digitizing seven glaciers three times and their means and STDs

Glacier	Region	Image code	Coastline length / Boundary length %	Area 1 km^2	Area 2 km^2	Area 3 km^2	Mean area km^2	STD %
1	EA	L7	24	4.2169	4.2432	4.2245	4.2282	0.32
2	WA	L8	0	73.0129	73.4527	73.5763	73.3473	0.40
3	WA	L9	52	136.8348	137.2223	137.2105	137.0892	0.16
4	EA	L10	100	217.5255	217.5044	217.4349	217.4883	0.02
5	WA	L11	28	645.3538	644.3441	645.6214	645.1064	0.10
6	EA	L12	0	1255.8587	1250.2902	1260.4463	1255.5317	0.41
7	WA	L13 & L14	23	3283.6716	3292.1492	3287.7966	3287.8725	0.13

https://doi.org/10.1017/aog.2023.75 Published online by Cambridge University Press

(misidentified features) and conceptual errors (e.g. glacier definition problems). These errors are the most influential uncertainties in assessing the accuracy of glacier outlines. Positional errors can be minimized if the satellite image is accurately orthorectified (Guo and others, 2015), and the Landsat images used in this study satisfy this requirement and thus can be recommended for use. Classification and conceptual errors, which are difficult to quantify (Racoviteanu and others, 2009) and are often influenced by the experience of glacier analysts, can be quite large in areas that are difficult to interpret from imagery (e.g. debris and snow cover, and the connection between glaciers and ice shelves). Therefore, glacier analysts need to be trained in glacier mapping to reduce the errors mentioned above. To minimize the impact of classification and conceptual errors in mapping glaciers, our work generally follows the GLIMS Analysis Tutorial (https://www.glims.org/MapsAndDocs/guides.html).

The issues of defining glaciers should be carefully considered when updating glacier outlines for a broader area. In this study, some glacier definitions refer to classification results from previous glacier inventories without additional rules of interpretation. For example, boundary locations of previous inventories were preserved at the connection of Greenland glaciers to the ice sheet. The interpretation of the boundary at glacier outlets in Antarctica follows the contrast variation of the images (as in RGI 6.0) with reference to the higher REMA contours (e.g. Fig. 10h). It is important to note here that the abrupt changes in optical contrast and contours are not consistent, as outlet glaciers can drain into ice shelves over considerable distances and lose front features which are generally included in glacier inventories in other regions. In other words, the bias in the definition of glaciers is caused by visual indecipherability. Therefore, the above glacier definition issue may be a topic for future discussion and resolution. One possible solution is to use lower contours to obtain the approximate extent of the glacier at the outlet, as they tend to be able to approach the location of clear fronts in other regions.

In Antarctica, the use of contrast-enhanced images to distinguish between glaciers and ice shelves can facilitate manual interpretation, but some enhancement methods inevitably diffuse the displayed glacier boundary by a few pixels, compromising detailed assessment of glacier extent. Identifying and calibrating glaciers by changing reference (enhanced) images and expending more effort would help alleviate these problems. In the study area, correct identification of ice-debris landforms and separation of glaciers from snow are still challenging. In this regard, we again emphasize the importance of alternately referencing multi-time images and using Google Earth to assist in visual interpretation of glaciers. Combining InSAR and optical data would be an appropriate procedure for identifying rock glaciers, as they have different criteria and are complementary (e.g. Villarroel and others, 2018). For example, one option would be to overlay the interferograms on optical satellite images in Google Earth to identify them by visually interpreting the landforms and their morphological features (e.g. Wang and others, 2017; Villarroel and others, 2018).

In the last decade and in the future, further optical data covering the study area, such as Sentinel-2 and Landsat 9, allow the mapping of large areas of glaciers on the periphery of the study area in a single day. In particular, the higher spatial resolution of Sentinel-2 (10 m, instead of 30 m for Landsat multispectral imagery) will help to improve the quality of glacier outlines; for example, debris-covered glaciers can be depicted more accurately. The shorter repeat intervals (5 days for Sentinel-2A and 2B in orbit) increase the opportunities to acquire snow- and cloud-free images from the end of the ablation period (Paul and others, 2016). However, coverage of Sentinel-2 and Landsat sensor is missing in the far north above 80°N in Greenland and northern Canada. We have noticed that the current USGS Earth Explorer provides dozens of OLI scenes located in this region, which are undoubtedly valuable data for glacier mapping.

Finally, we would like to emphasize that the cumbersome nature of this work, as well as the enormous amount of labor required, give a significant barrier to its promotion. We propose using the Google Earth Engine platform to help facilitate this process, such as filtering to select and composite the best images with fewer clouds and snow, calculating and segmenting band ratios, as well as processing raster and vector data. In addition, machine learning and deep learning techniques that have demonstrated good performance and great potential for rapid extraction of glacier boundaries may be able to reduce large manual efforts in this work and future study (e.g. Baumhoer and others, 2019; Lu and others, 2021; Chu and others, 2022).

6. Conclusion

In this work, we have illustrated and evaluated the possibilities for using new multi-source datasets and established techniques to handle glacier mapping challenges in complicated regions of Antarctica and Greenland, as well as update the inventories of GIC. In test scenarios, two schemes were considered as detailed demonstrations to map marine-terminating and land-terminating glacier boundaries, and glacier boundaries with ice shelves and sea ice. Glacier complexes were subsequently divided to obtain final glacier outlines and attributes, and their precision or uncertainty was evaluated qualitatively and quantitatively. Some visual comparisons with previous inventories indicate that the update effort has resulted in higher positioning accuracy of boundaries and more consistent and accurate rock areas for Antarctica. We used OLI (15 m) instead of the ETM+ (30 m) sensor to map higher-resolution glacier boundaries in Greenland and we used high-accuracy DEMs to generate well-performing watersheds. In particular, reliable multi-source data and integrated technologies support the reduction of uncertainty in the mapping process and mapping challenges such as debris cover, snow, shadows and delineation of watersheds.

We found that ice-shelf-terminating boundaries generally contribute more uncertainty to the mapped area of each glacier in Antarctica than marine-terminating or land-terminating boundaries by assessing the significance of changes (i.e. STD) in glacier area from multiple digitizations. A comparison with the ETM+ result of glacier mapping, under the rule of minimizing manual intervention and generalization differences, shows that the total area of selected glaciers mapped using our OLI method at 15 m resolution is approximately 3.1% smaller. These discussions imply that the impact of terminus types and substituted sensors on the glacier mapping results must be taken into account in polar GIC change analysis.

This work contributes to better understanding of the processes and challenges associated with creating and updating polar GIC inventories. It may also help in the establishment of accurate time-series inventories over a larger spatial and temporal range, allowing analysis of changes in the basic positions and attribute parameters of these glaciers. This work could be accomplished using more diverse sensors and datasets. The use of Google Earth Engine may help to reduce the large amount of manual workload required for the update process, allowing this work to be more generalized in the future.

Supplementary material. The supplementary material for this article can be found at https://doi.org/10.1017/aog.2023.75

Data. The glacier outlines in the case studies are available from the authors on request.

https://doi.org/10.1017/aog.2023.75 Published online by Cambridge University Press

Acknowledgements. This work was supported by the National Key Research and Development Program of China under grants 2021YFB3900105. We thank the support from the Fundamental Research Funds for the Central Universities. We thank the USGS for providing the satellite images and the LIMA, the NSIDC for providing the GLIMS glacier database and RGI 6.0, Antarctica/Greenland ice velocity maps, RAMP DEM and GIMP DEM, the University of Minnesota for providing REMA and ArcticDEM, the European Space Agency (ESA) for providing the Copernicus Sentinel-1 data, the ASF for providing the coherence images and the National Tibetan Plateau Data Center (TPDC) for providing the New Image Mosaic of Greenland. We would also like to thank Harold Lovell, the anonymous reviewer and the editors Luke Copland and Hester Jiskoot for their helpful and constructive comments that greatly helped improve the clarity of the paper.

References

Abermann J and Langley K (2022) Challenging the southern boundary of active rock glaciers in West Greenland. *Permafrost and Periglacial Processes* **33**(2), 129–133. doi: 10.1002/ppp.2139

Atwood DK, Meyer F and Arendt A (2010) Using L-band SAR coherence to delineate glacier extent. *Canadian Journal of Remote Sensing* **36**, S186–S195. doi: 10.5589/m10-014

Barella R and 8 others (2022) Combined use of Sentinel-1 and Sentinel-2 for glacier mapping: an application over Central East Alps. *Ieee Journal of Selected Topics in Applied Earth Observations and Remote Sensing* **15**, 4824–4834. doi: 10.1109/jstars.2022.3179050

Baumhoer CA, Dietz AJ, Kneisel C and Kuenzer C (2019) Automated extraction of Antarctic glacier and ice shelf fronts from Sentinel-1 imagery using deep learning. *Remote Sensing* **11**(21), 2529. doi: 10.3390/rs11212529

Berthling I (2011) Beyond confusion: rock glaciers as cryo-conditioned landforms. *Geomorphology* **131**(3–4), 98–106. doi: 10.1016/j.geomorph.2011.05.002

Bindschadler R and 8 others (2008) The Landsat image mosaic of Antarctica. *Remote Sensing of Environment* **112**(12), 4214–4226. doi: 10.1016/j.rse.2008.07.006

Bindschadler R and 17 others (2011) Getting around Antarctica: new high-resolution mappings of the grounded and freely-floating boundaries of the Antarctic ice sheet created for the International Polar Year. *Cryosphere* **5**(3), 569–588. doi: 10.5194/tc-5-569-2011

Bliss A, Hock R and Cogley JG (2013) A new inventory of mountain glaciers and ice caps for the Antarctic periphery. *Annals of Glaciology* **54**(63), 191–199. doi: 10.3189/2013AoG63A377

Bolch T, Menounos B and Wheate R (2010) Landsat-based inventory of glaciers in western Canada, 1985–2005. *Remote Sensing of Environment* **114**(1), 127–137. doi: 10.1016/j.rse.2009.08.015

Bolch T and 6 others (2013) Mass loss of Greenland's glaciers and ice caps 2003–2008 revealed from ICESat laser altimetry data. *Geophysical Research Letters* **40**(5), 875–881. doi: 10.1002/grl.50270

Bolch T, Rohrbach N, Kutuzov S, Robson BA and Osmonov A (2019) Occurrence, evolution and ice content of ice-debris complexes in the Ak-Shiirak, Central Tien Shan revealed by geophysical and remotely-sensed investigations. *Earth Surface Processes and Landforms* **44**(1), 129–143. doi: 10.1002/esp.4487

Brencher G, Handwerger AL and Munroe JS (2021) InSAR-based characterization of rock glacier movement in the Uinta Mountains, Utah, USA. *Cryosphere* **15**(10), 4823–4844. doi: 10.5194/tc-15-4823-2021

Burton-Johnson A, Black M, Fretwell PT and Kaluza-Gilbert J (2016) An automated methodology for differentiating rock from snow, clouds and sea in Antarctica from Landsat 8 imagery: a new rock outcrop map and area estimation for the entire Antarctic continent. *Cryosphere* **10**(4), 1665–1677. doi: 10.5194/tc-10-1665-2016

Chen Z and 6 others (2020) A new image mosaic of Greenland using Landsat-8 OLI images. *Science Bulletin* **65**(7), 522–524. doi: 10.1016/j.scib.2020.01.014

Cheng D and 6 others (2021) Calving Front Machine (CALFIN): glacial termini dataset and automated deep learning extraction method for Greenland, 1972-2019. *Cryosphere* **15**(3), 1663–1675. doi: 10.5194/tc-15-1663-2021

Chu XD and 5 others (2022) Glacier extraction based on high-spatial-resolution remote-sensing images using a deep-learning approach with attention mechanism. *Cryosphere* **16**(10), 4273–4289. doi: 10.5194/tc-16-4273-2022

Cook AJ, Vaughan DG, Luckman AJ and Murray T (2014) A new Antarctic Peninsula glacier basin inventory and observed area changes since the 1940s. *Antarctic Science* **26**(6), 614–624. doi: 10.1017/s0954102014000200

Frey H, Paul F and Strozzi T (2012) Compilation of a glacier inventory for the western Himalayas from satellite data: methods, challenges, and results. *Remote Sensing of Environment* **124**, 832–843. doi: 10.1016/j.rse.2012.06.020

Frezzotti M and Orombelli G (2014) Glaciers and ice sheets: current status and trends. *Rendiconti Lincei-Scienze Fisiche E Naturali* **25**(1), 59–70. doi: 10.1007/s12210-013-0255-z

Gardner AS and 15 others (2013) A reconciled estimate of glacier contributions to sea level rise: 2003 to 2009. *Science* **340**(6134), 852–857. doi: 10.1126/science.1234532

Granshaw FD and Fountain AG (2006) Glacier change (1958–1998) in the North Cascades National Park Complex, Washington, USA. *Journal of Glaciology* **52**(177), 251–256. doi: 10.3189/172756506781828782

Guo WQ and 10 others (2015) The second Chinese glacier inventory: data, methods and results. *Journal of Glaciology* **61**(226), 357–372. doi: 10.3189/2015JoG14J209

Haeberli W and 10 others (2006) Permafrost creep and rock glacier dynamics. *Permafrost and Periglacial Processes* **17**(3), 189–214. doi: 10.1002/ppp.561

He X and Zhou SQ (2022) An assessment of glacier inventories for the Third Pole Region. *Frontiers in Earth Science* **10**, 848007. doi: 10.3389/feart.2022.848007

Herreid S and Pellicciotti F (2020) The state of rock debris covering Earth's glaciers. *Nature Geoscience* **13**(9), 621. doi: 10.1038/s41561-020-0615-0

Hock R, de Woul M, Radic V and Dyurgerov M (2009) Mountain glaciers and ice caps around Antarctica make a large sea-level rise contribution. *Geophysical Research Letters* **36**(7), L07501. doi: 10.1029/2008gl037020

Hock R, Maussion F, Marzeion B and Nowicki S (2022) What is the global glacier ice volume outside the ice sheets?. *Journal of Glaciology* **69**(273), 204–210. doi: 10.1017/jog.2023.1

Howat IM, Negrete A and Smith BE (2014) The Greenland ice mapping project (GIMP) land classification and surface elevation data sets. *Cryosphere* **8**(4), 1509–1518. doi: 10.5194/tc-8-1509-2014

Howat I, Negrete A and Smith B (2015) MEaSUREs Greenland Ice Mapping Project (GIMP) Digital Elevation Model, Version 1.

Howat IM, Porter C, Smith BE, Noh MJ and Morin P (2019) The reference elevation model of Antarctica. *Cryosphere* **13**(2), 665–674. doi: 10.5194/tc-13-665-2019

Huber J, Cook AJ, Paul F and Zemp M (2017) A complete glacier inventory of the Antarctic Peninsula based on Landsat 7 images from 2000 to 2002 and other preexisting data sets. *Earth System Science Data* **9**(1), 115–131. doi: 10.5194/essd-9-115-2017

Hugonnet R and 10 others (2021) Accelerated global glacier mass loss in the early twenty-first century. *Nature* **592**(7856), 726. doi: 10.1038/s41586-021-03436-z

Huss M and Farinotti D (2012) Distributed ice thickness and volume of all glaciers around the globe. *Journal of Geophysical Research-Earth Surface* **117**, F04010. doi: 10.1029/2012jf002523

Janke JR, Bellisario AC and Ferrando FA (2015) Classification of debris-covered glaciers and rock glaciers in the Andes of central Chile. *Geomorphology* **241**, 98–121. doi: 10.1016/j.geomorph.2015.03.034

Jiskoot H, Juhlin D, St Pierre H and Citterio M (2012) Tidewater glacier fluctuations in central East Greenland coastal and Fjord regions (1980s-2005). *Annals of Glaciology* **53**(60), 35–44. doi: 10.3189/2012AoG60A030

Joughin I, Smith B, Howat I and Scambos T (2015) MEaSUREs Greenland Ice Sheet Velocity Map from InSAR Data, Version 2.

Ke LH and 5 others (2016) Compiling a new glacier inventory for southeastern Qinghai-Tibet Plateau from Landsat and PALSAR data. *Journal of Glaciology* **62**(233), 579–592. doi: 10.1017/jog.2016.58

Kienholz C, Hock R and Arendt AA (2013) A new semi-automatic approach for dividing glacier complexes into individual glaciers. *Journal of Glaciology* **59**(217), 925–937. doi: 10.3189/2013JoG12J138

Krieger L, Johnson E and Floricioiu D (2020a) A new drainage basin delineation for the southern Patagonian Ice Field based on TerraSAR-X velocities and TanDEM-X elevations. In *IEEE Latin American GRSS and ISPRS Remote Sensing Conference (LAGIRS)*, IEEE, pp. 441–444.

Krieger L, Floricioiu D and Neckel N (2020b) Drainage basin delineation for outlet glaciers of Northeast Greenland based on Sentinel-1 ice velocities and

TanDEM-X elevations. *Remote Sensing of Environment* **237**, 111483. doi: 10.1016/j.rse.2019.111483

Le Bris R, Paul F, Frey H and Bolch T (2011) A new satellite-derived glacier inventory for western Alaska. *Annals of Glaciology* **52**(59), 135–143. doi: 10.3189/172756411799096303

Lea JM, Mair DWF and Rea BR (2014) Instruments and methods evaluation of existing and new methods of tracking glacier terminus change. *Journal of Glaciology* **60**(220), 323–332. doi: 10.3189/2014JoG13J061

Lippl S, Vijay S and Braun M (2018) Automatic delineation of debris-covered glaciers using InSAR coherence derived from X-, C- and L-band radar data: a case study of Yazgyl Glacier. *Journal of Glaciology* **64**(247), 811–821. doi: 10.1017/jog.2018.70

Liu H, Jezek KC, Li B and Zhao Z (2015) Radarsat Antarctic Mapping Project Digital Elevation Model, Version 2.

Liu HX, Jezek KC and Li BY (1999) Development of an Antarctic digital elevation model by integrating cartographic and remotely sensed data: a geographic information system based approach. *Journal of Geophysical Research-Solid Earth* **104**(B10), 23199–23213. doi: 10.1029/1999jb900224

Lu YJ, Zhang Z and Huang DN (2020) Glacier mapping based on random forest algorithm: a case study over the Eastern Pamir. *Water* **12**(11), 3231. doi: 10.3390/w12113231

Lu YJ, Zhang Z, Shangguan DH and Yang JH (2021) Novel machine learning method integrating ensemble learning and deep learning for mapping debris-covered glaciers. *Remote Sensing* **13**(13), 2595. doi: 10.3390/rs13132595

Meier MF and 7 others (2007) Glaciers dominate Eustatic sea-level rise in the 21st century. *Science* **317**(5841), 1064–1067. doi: 10.1126/science.1143906

Molg N, Bolch T, Rastner P, Strozzi T and Paul F (2018) A consistent glacier inventory for Karakoram and Pamir derived from Landsat data: distribution of debris cover and mapping challenges. *Earth System Science Data* **10**(4), 1807–1827. doi: 10.5194/essd-10-1807-2018

Monnier S and Kinnard C (2015) Reconsidering the glacier to rock glacier transformation problem: New insights from the central Andes of Chile. *Geomorphology* **238**, 47–55. doi: 10.1016/j.geomorph.2015.02.025

Nuimura T and 12 others (2015) The GAMDAM glacier inventory: a quality-controlled inventory of Asian glaciers. *Cryosphere* **9**(3), 849–864. doi: 10.5194/tc-9-849-2015

Oerlemans J (2001) *Glaciers and Climate Change*. Rotterdam: A. A. Balkema Publishers.

Paul F and Andreassen LM (2009) A new glacier inventory for the Svartisen region, Norway, from Landsat ETM plus data: challenges and change assessment. *Journal of Glaciology* **55**(192), 607–618. doi: 10.3189/002214309789471003

Paul F and Kääb A (2005) *Perspectives on the production of a glacier inventory from multispectral satellite data in Arctic Canada: Cumberland Peninsula, Baffin Island*, Vol. 42, Cambridge University Press, pp. 59–66.

Paul F, Kääb A, Maisch M, Kellenberger T and Haeberli W (2002) *The new remote-sensing-derived Swiss glacier inventory: I. Methods*, Vol. 34, Cambridge University Press, pp. 355–361.

Paul F, Huggel C and Kaab A (2004) Combining satellite multispectral image data and a digital elevation model for mapping debris-covered glaciers. *Remote Sensing of Environment* **89**(4), 510–518. doi: 10.1016/j.rse.2003.11.007

Paul F and 9 others (2009) Recommendations for the compilation of glacier inventory data from digital sources. *Annals of Glaciology* **50**(53), 119–126. doi: 10.3189/172756410790595778

Paul F, Frey H and Le Bris R (2011) A new glacier inventory for the European Alps from Landsat TM scenes of 2003: challenges and results. *Annals of Glaciology* **52**(59), 144–152. doi: 10.3189/172756411799096295

Paul F and 19 others (2013) On the accuracy of glacier outlines derived from remote-sensing data. *Annals of Glaciology* **54**(63), 171–182. doi: 10.3189/2013AoG63A296

Paul F and 24 others (2015) The glaciers climate change initiative: methods for creating glacier area, elevation change and velocity products. *Remote Sensing of Environment* **162**, 408–426. doi: 10.1016/j.rse.2013.07.043

Paul F, Winsvold SH, Kaab A, Nagler T and Schwaizer G (2016) Glacier remote sensing using Sentinel-2. Part II: mapping glacier extents and surface facies, and comparison to Landsat 8. *Remote Sensing* **8**(7), 575. doi: 10.3390/rs8070575

Paul F and 10 others (2017) Error sources and guidelines for quality assessment of glacier area, elevation change, and velocity products derived from satellite data in the Glaciers cci project. *Remote Sensing of Environment* **203**, 256–275. doi: 10.1016/j.rse.2017.08.038

Pfeffer WT and 76 others (2014) The Randolph Glacier Inventory: a globally complete inventory of glaciers. *Journal of Glaciology* **60**(221), 537–552. doi: 10.3189/2014JoG13J176

Porter C and 28 others (2018) ArcticDEM, Version 3.

Racoviteanu AE, Paul F, Raup B, Khalsa SJS and Armstrong R (2009) Challenges and recommendations in mapping of glacier parameters from space: results of the 2008 Global Land Ice Measurements from Space (GLIMS) workshop, Boulder, Colorado, USA. *Annals of Glaciology* **50**(53), 53–69. doi: 10.3189/172756410790595804

Rastner P and 5 others (2012) The first complete inventory of the local glaciers and ice caps on Greenland. *Cryosphere* **6**(6), 1483–1495. doi: 10.5194/tc-6-1483-2012

Raup B and 5 others (2007) The GLIMS geospatial glacier database: A new tool for studying glacier change. *Global and Planetary Change* **56**(1–2), 101–110. doi: 10.1016/j.gloplacha.2006.07.018

Reinosch E, and 5 others (2021) Rock glacier inventory of the western Nyainqentanglha Range, Tibetan Plateau, supported by InSAR time series and automated classification. *Permafrost and Periglacial Processes* **32**(4), 657–672. doi: 10.1002/ppp.2117

RGI Consortium (2023) Randolph Glacier Inventory – a dataset of Global Glacier Outlines, Version 7.

Rignot E, Mouginot J and Scheuchl B (2017) MEaSUREs InSAR-Based Antarctica Ice Velocity Map, Version 2.

Rivera A, Bown F, Casassa G, Acuna C and Clavero J (2005) Glacier shrinkage and negative mass balance in the Chilean Lake District (40 degrees S). *Hydrological Sciences Journal-Journal Des Sciences Hydrologiques* **50**(6), 963–974. doi: 10.1623/hysj.2005.50.6.963

Rudolph EM, Meiklejohn KI, Hansen CD, Hedding DW and Nel W (2018) Rock glaciers in the Jutulsessen, Dronning Maud Land, East Antarctica. *Polish Polar Research* **39**(1), 1–17. doi: 10.24425/118736

Strelin JA and Sone T (1998) Rock glaciers on James Ross Island, Antarctica. In *Permafrost–Seventh International Conference (Proceedings)*, Vol. 55, pp. 1027–1033.

Strozzi T and 8 others (2020) Monitoring rock glacier kinematics with satellite synthetic aperture radar. *Remote Sensing* **12**(3), 559. doi: 10.3390/rs12030559

Tanarro LM, Palacios D, Zamorano JJ and Andres N (2018) Proposal for geomorphological mapping of debris-covered and rock glaciers and its application to Trollaskagi Peninsula (Northern Iceland). *Journal of Maps* **14**(2), 692–703. doi: 10.1080/17445647.2018.1539417

Villarroel CD, Beliveau GT, Forte AP, Monserrat O and Morvillo M (2018) DInSAR for a regional inventory of active rock glaciers in the Dry Andes mountains of Argentina and Chile with Sentinel-1 Data. *Remote Sensing* **10**(10), 1588. doi: 10.3390/rs10101588

Wang XW and 5 others (2017) Mapping and inventorying active rock glaciers in the northern Tien Shan of China using satellite SAR interferometry. *Cryosphere* **11**(2), 997–1014. doi: 10.5194/tc-11-997-2017

Winsvold SH and 5 others (2018) Using SAR satellite data time series for regional glacier mapping. *Cryosphere* **12**(3), 867–890. doi: 10.5194/tc-12-867-2018

Winsvold SH, Kaab A and Nuth C (2016) Regional glacier mapping using optical satellite data time series. *Ieee Journal of Selected Topics in Applied Earth Observations and Remote Sensing* **9**(8), 3698–3711. doi: 10.1109/jstars.2016.2527063

Wulder MA, Masek JG, Cohen WB, Loveland TR and Woodcock CE (2012) Opening the archive: how free data has enabled the science and monitoring promise of Landsat. *Remote Sensing of Environment* **122**, 2–10. doi: 10.1016/j.rse.2012.01.010

Zemp M and 14 others (2019) Global glacier mass changes and their contributions to sea-level rise from 1961 to 2016. *Nature* **568**(7752), 382. doi: 10.1038/s41586-019-1071-0

Zhang XF and 7 others (2021) Detecting rock glacier displacement in the central Himalayas using multi-temporal InSAR. *Remote Sensing* **13**(23), 4738. doi: 10.3390/rs13234738

https://doi.org/10.1017/aog.2023.75 Published online by Cambridge University Press